IL NUOVO CIMENTO VOL. 18 B, N. 1 11 Novembre 1973

The Band-Gap Excitons in Gallium Selenide (*).

E. MOOSER and M. SCHLÜTER (**)

Laboratoire de Physique Appliquée, Ecole Polytechnique Federale de Lausanne - Lausanne

(ricevuto il 31 Luglio 1973)

Summary. — Absorption and reflexion spectra of GaSe near the fundamental gap are interpreted in terms of pseudopotential band calculations. Selection rules for the direct optical valence-to-conduction band transitions are derived. Valence band mixing induced by spin-orbit coupling is invoked to explain the low observed probability for transitions in light polarized perpendicular to the crystal c-axis. The spectra of the excitons associated with the direct gap are discussed in the ellipsoidal effective-mass approximation. Corrective terms are added to account for the observed exchange splitting of the exciton ground state. Field-free spectra as well as spectra modified by the presence of magnetic fields parallel and perpendicular to c are considered. The magneto-Stark effect which gives rise to a mixing of the $2s$ and $2p_y$ states and thus renders the $2p_y$ state visible affords determination of the anisotropy parameter. The value of this parameter as well as those of the components parallel and perpendicular to c of the reduced effective masses show that the electronic states in GaSe are nearly isotropic. This is in good agreement with the results of the pseudopotential band calculations which clearly demonstrate the three-dimensional character of valence and conduction bands.

1. – Introduction.

As early as 1958 FIELDING, FISCHER and MOOSER [1] observed an exciton near the fundamental absorption edge of GaSe. Later it was found that

(*) Supported in part by the Swiss National Science Foundation.

(**) Present address: c/o Professor M. L. COHEN, Physics Department, University of California, Berkeley, Cal. 94720.

(1) P. FIELDING, G. FISCHER and E. MOOSER: *Journ. Phys. Chem. Sol.*, **8**, 434 (1959).

the layer structure of this compound gives rise to a specific growth habit in crystals grown by sublimation or by iodine transport: large but very thin flakes form ([2,3]) which can, without machining, be used for optical-absorption measurements. Practically strain-free samples are thus obtained which exhibit well-resolved exciton spectra. Moreover, early absorption measurements ([4]) already indicated that the fundamental transition is allowed only if the polarization vector $\boldsymbol{E}$ of the incident light is perpendicular to the plane of the layers. If $\boldsymbol{E}$ is in this plane the transition gives rise to a small absorption only and it is possible, therefore, in a suitable geometry to carry out absorption experiments well beyond the fundamental edge. A series of magneto-optical absorption measurements ([5-7]) was thus performed which led to a number of most interesting theoretical investigations ([8-12]) on the behaviour of Landau levels in the presence of a Coulombic electron-hole interaction. All these investigations were, however, only concerned with the magneto-optical spectrum at energies above the ionization limit of the exciton and in high magnetic fields. Recently BREBNER ([13]) has proposed an interpretation of the low-field magneto-absorption in the lowest exciton states and on the basis of his interpretation suggests a possible correlation between the low- and the high-field observations. The rather difficult problem of correlating the zero-field exciton states with the high-field Landau levels has been discussed theoretically by SHINADA *et al.* ([14]) and by BASSANI and BALDERESCHI ([15]). It follows from these discussions that Brebner's identification of some of the observed lines is probably in error and we therefore propose an alternative explanation of the same experimental data ([7,13]), restricting ourselves to low fields and low energies only.

([2]) R. NIETSCHE, H. U. BOELSTERLI and M. LICHTENSTEIGER: *Journ. Phys. Chem. Sol.*, **21**, 199 (1961).
([3]) H. U. BOELSTERLI and E. MOOSER: *Helv. Phys. Acta*, **35**, 538 (1962).
([4]) J. L. BREBNER: *Journ. Phys. Chem. Sol.*, **25**, 1427 (1964).
([5]) J. HALPERN: *Proceedings of the International Conference on Semiconductors* (Kyoto, 1966), p. 180.
([6]) K. AOYAGI, A. MISU, G. KUWABARA, Y. NISHINA, S. KURITA, T. FUKUROI, O. AKIMOTO, H. HASEGAWA, M. SHINADA and S. SUGANO: *Proceedings of the International Conference on Semiconductors* (Kyoto, 1966), p. 174.
([7]) J. L. BREBNER, J. HALPERN and E. MOOSER: *Helv. Phys. Acta*, **40**, 385 (1967).
([8]) A. BALDERESCHI and F. BASSANI: *Phys. Rev. Lett.*, **19**, 66 (1967).
([9]) A. BALDERESCHI and F. BASSANI: *Proceedings of the International Conference on the Physics of Semiconductors*, Vol. **1** (Moscow, 1968), p. 280.
([10]) L. FRITSCHE: *Phys. Stat. Sol.*, **34**, 195 (1969).
([11]) L. FRITSCHE and F. D. HEIDT: *Phys. Stat. Sol.*, **35**, 987 (1969).
([12]) O. AKIMOTO and H. HASEGAWA: *Journ. Phys. Soc. Japan*, **22**, 181 (1966).
([13]) J. L. BREBNER: *Canad. Journ. Phys.*, **51**, 497 (1973).
([14]) M. SHINADA, O. AKIMOTO, H. HASEGAWA and K. TANAKA: *Journ. Phys. Soc. Japan*, **28**, 975 (1970).
([15]) F. BASSANI and A. BALDERESCHI: *Surface Sci.*, **37**, 304 (1973).

The limitations of the earlier interpretations are at least partly due to the fact that only band calculations ([16-18]) neglecting the interlayer interaction were available at the time. Such band calculations correspond to two-dimensional crystals and among other things they cannot, therefore, account for the fact that the observed exciton series follows very closely the $1/n^2$ law typical of three-dimensional Wannier excitons and not the $1/(2n-1)^2$ law expected ([19,20]) for two-dimensional excitons. The problem of the Wannier exciton in anisotropic structures has since been treated theoretically by DÉVERIN ([21,22]) and by BALDERESCHI and DIAZ ([23]).

The three-dimensional character of the excitons in GaSe is confirmed by the fine structure ([24]) of the exciton ground state. Indeed, it was possible to interpret ([25]) some of the features of this fine structure in terms of the different possibilities of stacking layers of GaSe on top of each other, *i.e.* in terms of the different polytypes in which GaSe is known to crystallize.

Additional structure of the exciton states was found to depend strongly on the polarization of the incident radiation ([24,26]). In fact two different exciton series were found one each for $\boldsymbol{E}$ parallel and perpendicular to the layer plane. While the ground states of the two series differ by about 2 meV, corresponding excited states rapidly merge and can no longer be resolved: the two series converge towards the same series limit.

A rather unexpected experimental result ([27]) showed that the direct gap with which the excitons are associated is not the lowest one: there exists an indirect gap at an energy several tens of meV below the direct one. The corresponding indirect transition has the same polarization dependence as the direct transition and therefore is visible only in thick samples with light incident along the layer plane and with the polarization vector perpendicular to this plane. A lowest indirect gap had been predicted on theoretical grounds by KAMIMURA ([18]). Moreover, KAMIMURA, NAKAO and NISHINA ([28]) have reported on a two-dimensional indirect exciton, but recent

---

([16]) F. BASSANI and G. PASTORI PARRAVICINI: *Nuovo Cimento*, **50** B, 95 (1967).
([17]) H. KAMIMURA and K. NAKAO: *Proceedings of the International Conference on Semiconductors* (Kyoto, 1966), p. 27.
([18]) H. KAMIMURA and K. NAKAO: *Journ. Phys. Soc. Japan*, **24**, 1313 (1968).
([19]) H. J. RALPH: *Solid State Comm.*, **3**, 303 (1965).
([20]) M. SHINADA and S. SUGANO: *Journ. Phys. Soc. Japan*, **21**, 1936 (1966).
([21]) J. A. DÉVERIN: *Helv. Phys. Acta*, **42**, 397 (1969).
([22]) J. A. DÉVERIN: *Nuovo Cimento*, **63** B, 1 (1969).
([23]) A. BALDERESCHI and M. G. DIAZ: *Nuovo Cimento*, **68** B, 217 (1970).
([24]) J. L. BREBNER, J. HALPERN and E. MOOSER: *Helv. Phys. Acta*, **40**, 385 (1967).
([25]) J. L. BREBNER and E. MOOSER: *Phys. Lett.*, **24** A, 274 (1967).
([26]) A. BOURDON and F. KHELLADI: *Solid State Comm.*, **9**, 1715 (1971).
([27]) E. AULICH, J. L. BREBNER and E. MOOSER: *Phys. Stat. Sol.*, **31**, 129 (1969).
([28]) H. KAMIMURA, K. NAKAO and Y. NISHINA: *Phys. Rev. Lett.*, **22**, 1379 (1969).

three-dimensional band calculations ([29]) cast some doubt upon these results.

In view of the current investigations on radiative exciton recombination in GaSe ([30-34]) the presence of an indirect gap below the exciton ground state is of particular interest. On the grounds of their measurements on stimulated band edge emission NAHORY *et al.* ([30]) actually reach the conclusion that there is no low-lying indirect gap in GaSe. In contrast to this, Schlüter's ([29]) band calculations lend support to its existence. Above all, however, these calculations afford a detailed interpretation of the direct-gap excitons and of their dependence on the polarization of the incident light and on an applied magnetic field. It is the aim of the present paper to elaborate this interpretation and thus to come to an identification of the observed exciton states.

Since our interpretation is at variance with that of BREBNER ([13]) and in order to facilitate an assessment of their respective merits some of the features of GaSe are discussed in detail here. Thus in Sect. **2** we dwell upon the structure and the different polytypes in so far as their knowledge is necessary for the understanding of the exciton series. Section **3** is devoted to a review of the main results of the band calculations and of the selection rules for the band-to-band transitions which can be derived from it. In Sect. **4** a brief outline is given of the effective-mass approximation of excitons in uniaxial crystals. The influence of spin-orbit coupling and exchange upon the exciton levels is studied. From a perturbation treatment similar to that used by WHEELER and DIMMOCK ([35]) for CdSe the exciton energies in a magnetic field are evaluated. In Sect. **5**, which contains some new experimental results, a detailed comparison between experiment and theory is given. This comparison yields new information about the reduced effective exciton masses and about the electronic anisotropy of GaSe.

2. – The crystal structure of GaSe.

The crystals of GaSe consist of rather loose stacks of covalently bonded layers each of which contains four monoatomic sheets in the sequence Se-Ga-Ga-Se. If we mark the three possible positions of a close-packed sheet within a three-dimensional close-packing by a, b and c if the sheet contains anions and by α, β and γ if it contains cations, a layer of GaSe can be described *e.g.* by $a\beta\beta a$.

([29]) M. SCHLÜTER: *Nuovo Cimento*, **13** B, 313 (1973).
([30]) R. E. NAHORY, K. L. SHAKLEE, R. F. LEHENY and J. C. DEWINTER: *Solid State Comm.*, **9**, 1107 (1971).
([31]) T. UGUMORI, K. MASUDA and S. NAMBA: *Phys. Lett.*, **38** A, 117 (1972).
([32]) J. P. VOITCHOVSKY and E. MOOSER: *Helv. Phys. Acta*, **45**, 877 (1972).
([33]) A. MERCIER, E. MOOSER and J. P. VOITCHOVSKY: *Journ. Luminescence*, **7**, 241 (1973).
([34]) T. UGUMORI, K. MASUDA and S. NAMBA: *Solid State Comm.*, **12**, 389 (1973).
([35]) R. G. WHEELER and J. O. DIMMOCK: *Phys. Rev.*, **125**, 1805 (1962).

Its space group is D_{3h}^1 and its hexagonal unit cell contains two molecules. The two sheets of Ga atoms within each layer are stacked « *a* over *a* » and we will see below that this stacking is the result of the formation of covalent Ga-Ga bonds.

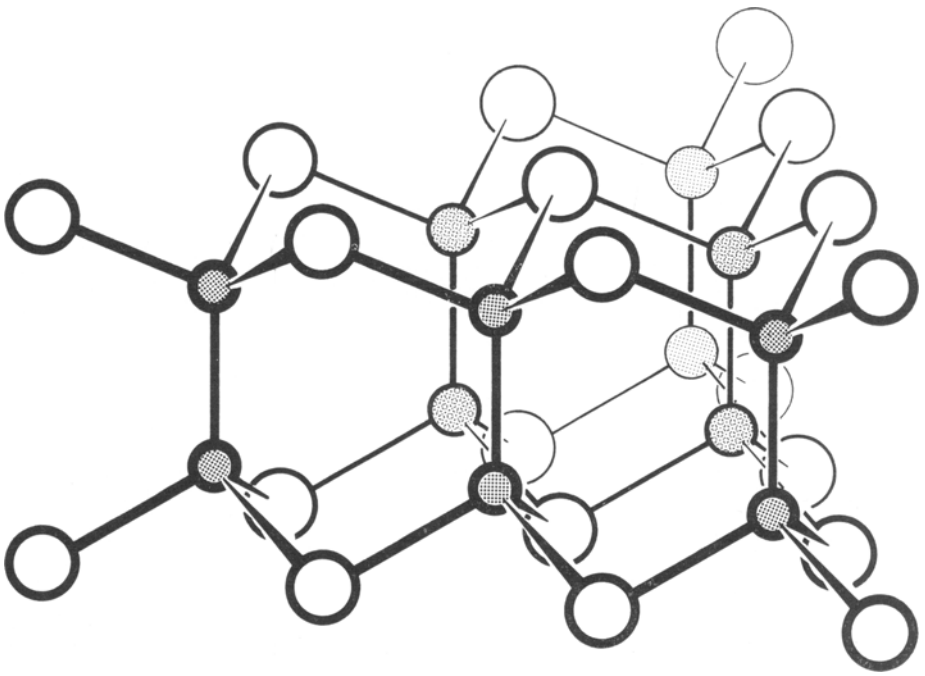

Fig. 1. – A layer of GaSe. The large circles represent the Se atoms, the small ones the Ga atoms.

In Fig. 1 a layer of GaSe is represented and one recognizes that each Ga atom has one Ga and three Se neighbours. The Se atoms have three neighbours only within the same layer. However, in the crystal each Se atom acquires three additional Se neighbours, in the adjacent layer at a distance of about $d_{Se\text{-}Se} = 3.6$ Å, typical for van der Waals bonding. The co-ordination of the Se atoms of each layer by three Se atoms of the neighbouring layer corresponds to « *a* over *b* » interlayer stacking. Although the different modifications of GaSe distinguish themselves by different stacking sequences, the interlayer « *a* over *b* » stacking and the distance $d_{Se\text{-}Se}$ remain unchanged within experimental accuracy.

2'1. *The β-modification.* – This modification is currently found in GaS [36] and much less frequently in transport reacted flakes of GaSe [25,37]. In terms

[36] H. HAHN and G. FRANK: *Zeits. anorg. allg. Chem.*, **278**, 340 (1955).
[37] F. JELLINEK and H. HAHN: *Zeits. Naturforsch.*, **16**, 713 (1961).

of the stacking symbols introduced above it is described by

$$\ldots a\beta\beta ab\alpha\alpha ba\beta\beta a \ldots .$$

Its space group is D^4_{6h} and its hexagonal unit cell contains four molecules. The c-axis runs perpendicular to the layer plane and extends over two layers. Each layer of β-GaSe can be brought into coincidence with one of its neighbouring layers by a translation $\tau = \pm c/2$ and a rotation in the plane of the layer through 60°. This rotation is responsible for the relatively high stacking fault energy observed in β-GaSe ([38]) which prevents release of residual strain and thus probably is responsible for the poor resolution of the exciton spectra of β-samples (see Fig. 9 below).

2·2. *The γ and ε modifications.* – All Bridgman and most transport grown samples contain intimate mixtures of γ- and ε-stacking. The two modifications will therefore be discussed simultaneously here. While the stacking sequence

$$\ldots a\beta\beta ab\gamma\gamma bc\alpha\alpha ca\beta\beta a \ldots$$

of the γ-modification is reminiscent of cubic close-packing, that

$$\ldots a\beta\beta ab\gamma\gamma ba\beta\beta a \ldots$$

of the ε-type derives from hexagonal close-packing. The corresponding space groups are C^5_{3v} and D^1_{3h} respectively. In both cases hexagonal unit cells can be defined whose c-axes are perpendicular to the layer plane. The cell of the γ-modification contains six molecules and extends over three layers, that of the ε-modification has four molecules and embraces two layers.

In both modifications a layer can be transformed into one of its neighbours by a translation. Unlike the β-crystals, glide stacking faults therefore have a very small energy only ([38]). Moreover (hypothetical) introduction of ordered stacking faults transforms the γ- into the ε-modification and *vice versa*. This is the reason why transport reacted flakes normally contain statistical mixtures of the two stacking types. Indeed, such flakes grow around screw dislocations running along c and having rather large ($(500 \div 1000)$ Å) Burgers vectors ([3]). To release the strain near the dislocation, slip occurs which produces statistically distributed glide stacking faults of the type described above.

3. – Band structure and optical transition in GaSe.

3·1. *The β-modification.* – The energy bands of β-GaSe along the main symmetry axes calculated ([29]) on the basis of the empirical pseudopotential ap-

([38]) Z. S. BASINSKI, D. B. DOVE and E. MOOSER: *Helv. Phys. Acta*, **34**, 373 (1961).

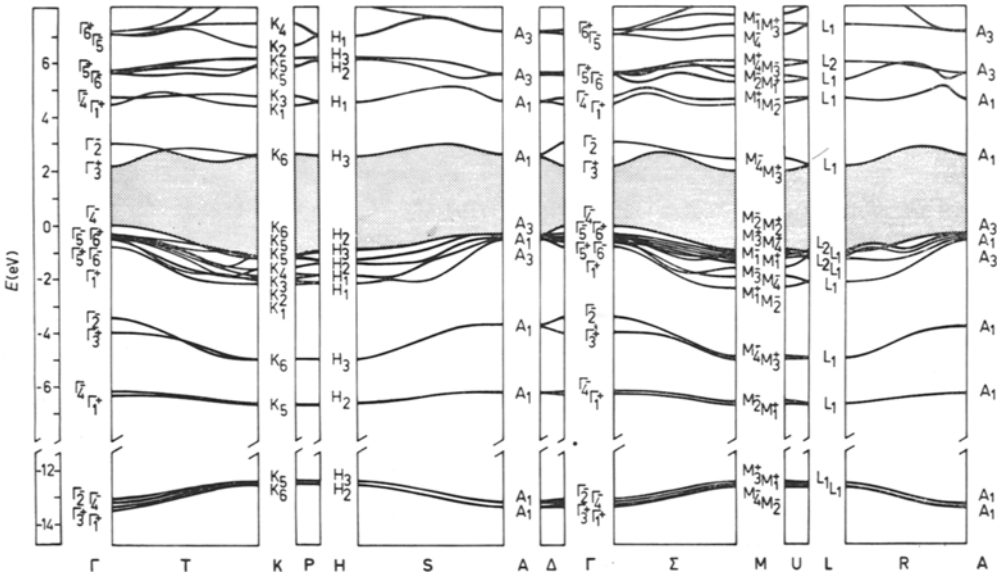

Fig. 2. – The band structure of GaSe (after SCHLÜTER [29]).

proach are plotted in Fig. 2. The calculations were carried out on the β-modification for reasons of economy: among the three known modifications, β-GaSe has the highest symmetry.

According to Fig. 2 the direct gap with which the exciton series of interest here are associated occurs at the centre Γ of the Brillouin zone, the top of the valence band having the symmetry Γ_4^- and the (relative) minimum of the conduction band that Γ_3^+. In Table I the selection rules are listed for direct

TABLE I (*). – *Selection rules for direct dipole transitions between the states Γ_i of the group D_{6h}^4.* The polarization vector $\boldsymbol{E} \parallel c$ belong to Γ_2^-, that $\boldsymbol{E} \perp c$ to Γ_5^-.

Initial state	Final state accessible with	
	$\boldsymbol{E} \perp c$	$\boldsymbol{E} \parallel c$
$\Gamma_1^\pm$	$\Gamma_5^\mp$	$\Gamma_2^\mp$
$\Gamma_2^\pm$	$\Gamma_5^\mp$	$\Gamma_1^\mp$
$\Gamma_3^\pm$	$\Gamma_6^\mp$	$\Gamma_4^\mp$
$\Gamma_4^\pm$	$\Gamma_6^\mp$	$\Gamma_3^\mp$
$\Gamma_5^\pm$	$\Gamma_1^\mp, \Gamma_2^\mp, \Gamma_6^\mp$	$\Gamma_5^\mp$
$\Gamma_6^\pm$	$\Gamma_3^\mp, \Gamma_4^\mp, \Gamma_5^\mp$	$\Gamma_6^\mp$

(*) The group-theoretical symbols used throughout this article are taken from KOSTER, DIMMOCK, WHEELER and STATZ [39].

(39) G. F. KOSTER, J. O. DIMMOCK, R. G. WHEELER and H. STATZ: *Properties of the Thirty-Two Point Groups* (Cambridge, Mass., 1963).

dipole transitions between states transforming according to the irreducible representations Γ_i of the group D_{6h}^4 and one recognizes that the transition $\Gamma_4^- \to \Gamma_3^+$ is allowed only for light whose polarization vector $\boldsymbol{E}$ is parallel to the c-axis of the crystal.

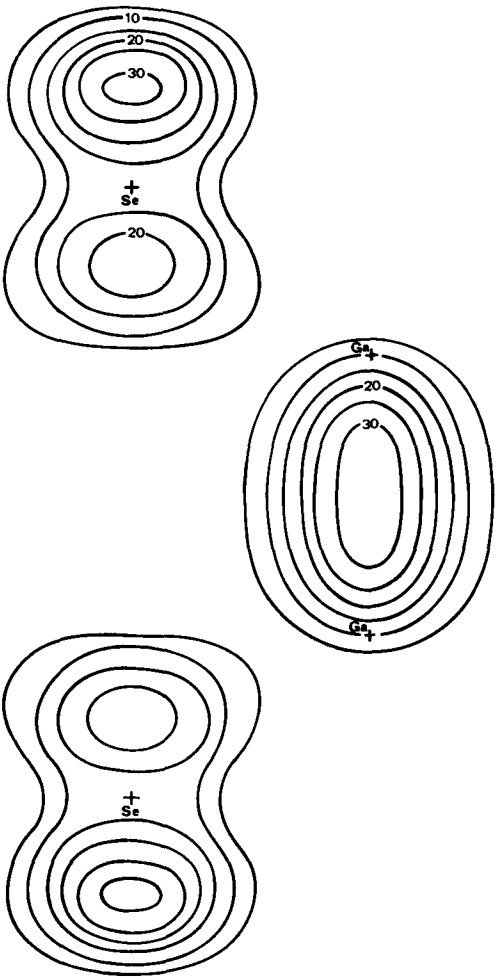

Fig. 3. – The spatial distribution of the electrons contained in the valence band pair Γ_1^+, Γ_4^- (after SCHLÜTER [29]).

On the basis of his band calculations SCHLÜTER [29] has evaluated the pseudo-densities of the valence electrons in the crystals. Thus Fig. 3 shows the distribution of the electrons contained in the valence band pair Γ_1^+, Γ_4^- around the four atoms per unit cell and per layer lying in the (110)-plane. As seen from this contour map the uppermost valence bands are formed by the bonding states corresponding to the Ga-Ga bond. A similar plot related to the distribution

of the electrons in the (hypothetically filled) lowest conduction band pair Γ_3^+, Γ_2^- is reproduced on Fig. 4. Obviously these two bands contain the antibonding states of the Ga-Ga bonds and one readily understands why on the basis of orbital symmetry alone only dipole transitions with $\boldsymbol{E} \parallel c$ are allowed.

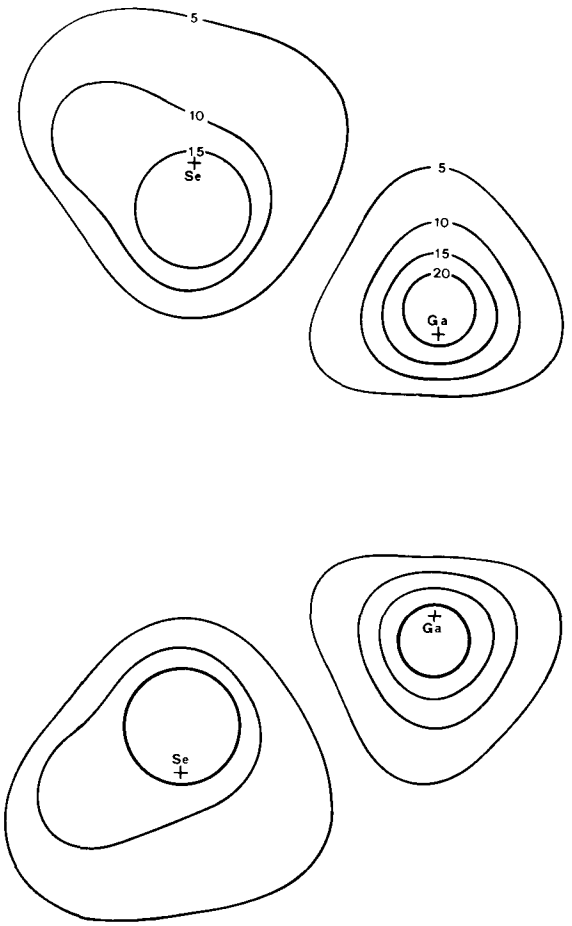

Fig. 4. – The spatial distribution of the electrons contained in the (hypothetically) filled conduction band pair Γ_3^+, Γ_2^- (after SCHLÜTER).

Experiment [4] confirms that light of this polarization is strongly absorbed in GaSe at energies above the band gap. However, there is in this region also an absorption for $\boldsymbol{E} \perp c$, which is only about one to two orders of magnitude weaker [4] than that for $\boldsymbol{E} \parallel c$, and which can be understood if in addition to the orbital symmetry one also considers the spin symmetry. This is best done by going into the double group $\bar{D}_{6h}^4 = D_{6h}^4 \times D^{(\frac{1}{2})}$, where $D^{(\frac{1}{2})}$ is the two-dimensional representation of the Pauli spinors. In Table IV the correspondence is given

TABLE II. – *Selection rules for direct dipole transitions between the states of the double group* $\bar{D}^4_{6h}$.

Initial state	Final state accessible with	
	$\boldsymbol{E} \perp c$	$\boldsymbol{E} \parallel c$
$\Gamma_7^{\pm}$	$\Gamma_7^{\mp}, \Gamma_9^{\mp}$	$\Gamma_7^{\mp}$
$\Gamma_8^{\pm}$	$\Gamma_8^{\mp}, \Gamma_9^{\mp}$	$\Gamma_8^{\mp}$
$\Gamma_9^{\pm}$	$\Gamma_7^{\mp}, \Gamma_8^{\mp}$	$\Gamma_9^{\mp}$

between the representations of the single group and the extra representations of the double group and one recognizes that at the Γ-point the symmetries of the highest valence and lowest conduction bands go from Γ_4^- to Γ_8^- and from Γ_3^+ to Γ_8^+ respectively. The corresponding selection rules (Table II) admit a dipole transition for $\boldsymbol{E} \perp c$. However, since this transition is only spin-allowed and since the polarization operator does not operate on spin, the experimentally observed absorption for $\boldsymbol{E} \perp c$ is indicative of the presence in GaSe of spin-orbit coupling. According to the band structure shown in Fig. 2 valence and conduction bands of GaSe are not orbitally degenerate at Γ. Spin-orbit coupling therefore results from interband mixing and thus is relatively weak. The mixing occurs between the valence band Γ_4^- and one (Γ_6^-) of the four closely spaced bands Γ_5^+, Γ_5^-, Γ_6^+ and Γ_6^- which are estimated to lie about 500 meV below Γ_4^-. Indeed in the double group Γ_4^- becomes Γ_8^- and Γ_6^- goes into $\Gamma_8^- + \Gamma_9^-$, so that mixing is possible. Interband mixing of the conduction band can be neglected because the separation between this band and any other band of appropriate symmetry is too large.

The p_x- and p_y-like character of the bands $\Gamma_5^{\pm}$ and $\Gamma_6^{\pm}$ ([29])—x and y define the layer plane—readily explains why the proposed mixing gives rise to a finite transition probability for $\boldsymbol{E} \perp c$.

The $\boldsymbol{k}$-dependence near the Γ-point of the corresponding matrix element M_{vc} is outlined schematically in Fig. 5 which shows that the transition for $\boldsymbol{E} \perp c$ is neither *allowed* nor *forbidden* in the usual sense of these terms.

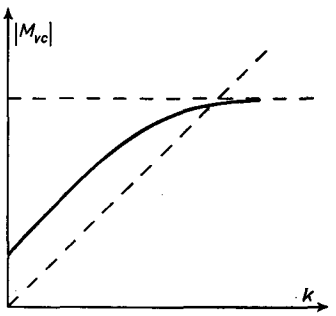

Fig. 5. – The matrix element M_{vc} for interband transitions with light polarized perpendicular to c (schematic).

The results of the above discussion relate to β-GaSe. This should not, however, deter us from applying them, with minor modifications, to the interpretation of the best experimental data ([7,13]) available at present which was invariably obtained on samples containing mixed γ-, ε-stacking. Thus we first of all note that the three modifications of GaSe have very nearly the same thermodynamical stability: they may be found side by side on the same vapour-grown sample. Moreover, it follows from optical-absorption measurements ([25,27]) that to within better than 0.2 meV the γ- and ε-types have the same direct gap and that the gap of β-GaSe is only 50 meV wider. Although some of the band degeneracies found in the β-type may be lifted in either the γ- or the ε-modidification, this lifting and any possible band shifts will be of the order of 50 meV only. No basic differences between the band structures of the different modifications are, therefore, expected. In particular, the selection rules for optical transitions near the fundamental edge are conserved. We will prove this for the case of highest interest here, *i.e.* for the selection rules relating to a single layer only.

3·2. *Single layer.* – Since the interlayer interaction in GaSe is relatively small and since the electron densities are highest within a layer, the Bloch functions in all modifications are essentially determined by the symmetry D^1_{3h} of a single layer. The discussion of the excitons in Sect. 4 will therefore be carried out in terms of the group D^1_{3h} and of those C^1_{3h} and C^1_s deriving from it when a magnetic field is applied parallel ($\boldsymbol{H} = (0, 0, H_z)$) and perpendicular ($\boldsymbol{H} = (H_x, 0, 0)$) to the c-axis. To account for spin effects the corresponding double groups $\bar{D}^1_{3h}$, $\bar{C}^1_{3h}$ and $\bar{C}^1_s$ are considered. In Table III the compatibility relations between representations of these groups are listed and Tables IV *a*)-IV *d*) give the relations between the single-group representations and the extra representations of the double groups.

TABLE III. – *Compatibility relations between representations of the groups* $\bar{D}^4_{6h}$, $\bar{D}^1_{3h}$, $\bar{C}^1_{3h}$ *and* $\bar{C}^1_s$.

	$\boldsymbol{H}$	Group	Single-group representations											
β-GaSe	0	$\bar{D}^4_{6h}$	Γ_1^+	Γ_1^-	Γ_2^+	Γ_2^-	Γ_3^+	Γ_3^-	Γ_4^+	Γ_4^-	Γ_5^+	Γ_5^-	Γ_6^+	Γ_6^-
Single layer	0	$\bar{D}^1_{3h}$	Γ_1	Γ_3	Γ_2	Γ_4	Γ_4	Γ_2	Γ_3	Γ_1	Γ_5	Γ_6	Γ_6	Γ_5
	H_z	$\bar{C}^1_{3h}$	Γ_1	Γ_4	Γ_1	Γ_4	Γ_4	Γ_1	Γ_4	Γ_1	$\Gamma_5+\Gamma_6$	$\Gamma_2+\Gamma_3$	$\Gamma_2+\Gamma_3$	$\Gamma_5+\Gamma_6$
	H_x	$\bar{C}^1_s$	Γ_1	Γ_2	Γ_2	Γ_1	Γ_1	Γ_2	Γ_2	Γ_1	$\Gamma_1+\Gamma_2$	$\Gamma_1+\Gamma_2$	$\Gamma_1+\Gamma_2$	$\Gamma_1+\Gamma_2$

	$\boldsymbol{H}$	Group	Extra representations of double group					
β-GaSe	0	$\bar{D}^4_{6h}$	Γ_7^+	Γ_7^-	Γ_8^+	Γ_8^-	Γ_9^+	Γ_9^-
Single layer	0	$\bar{D}^1_{3h}$	Γ_7	Γ_8	Γ_8	Γ_7	Γ_9	Γ_9
	H_z	$\bar{C}^1_{3h}$	$\Gamma_7+\Gamma_8$	$\Gamma_9+\Gamma_{10}$	$\Gamma_9+\Gamma_{10}$	$\Gamma_7+\Gamma_8$	$\Gamma_{11}+\Gamma_{12}$	$\Gamma_{11}+\Gamma_{12}$
	H_x	$\bar{C}^1_s$	$\Gamma_3+\Gamma_4$	$\Gamma_3+\Gamma_4$	$\Gamma_3+\Gamma_4$	$\Gamma_3+\Gamma_4$	$\Gamma_3+\Gamma_4$	$\Gamma_3+\Gamma_4$

In β-GaSe valence and conduction bands form pairs Γ_1^+, Γ_4^- and Γ_3^+, Γ_2^-, the energy separation within each pair being a measure for the interlayer interaction ([29]). In the single layer these pairs are replaced by the valence and conduction bands Γ_1 and Γ_4 respectively which at Γ are nondegenerate. The product $\Gamma_1 \times \Gamma_4$ belongs to the representation Γ_4 of D_{3h}^1 and, since the polarization

TABLE IV. – *Relations between representations of the single groups D_{6h}^4, D_{3h}^1, C_{3h}^1 and C_s^1 and the extra representations of the corresponding double groups.*

a) D_{6h}^4						
single group	$\Gamma_1^\pm$	$\Gamma_2^\pm$	$\Gamma_3^\pm$	$\Gamma_4^\pm$	$\Gamma_5^\pm$	$\Gamma_6^\pm$
double group	$\Gamma_7^\pm$	$\Gamma_7^\pm$	$\Gamma_8^\pm$	$\Gamma_8^\pm$	$\Gamma_7^\pm + \Gamma_9^\pm$	$\Gamma_8^\pm + \Gamma_9^\pm$
b) D_{3h}^1						
single group	Γ_1	Γ_2	Γ_3	Γ_4	Γ_5	Γ_6
double group	Γ_7	Γ_7	Γ_8	Γ_8	$\Gamma_7 + \Gamma_9$	$\Gamma_8 + \Gamma_9$
c) C_{3h}^1						
single group	Γ_1	Γ_2	Γ_3	Γ_4	Γ_5	Γ_6
double group	Γ_7	Γ_{11}	Γ_{10}	Γ_9	Γ_{12}	Γ_8
d) C_s^1						
single group	Γ_1	Γ_2				
double group	Γ_3	Γ_4				

vectors $\boldsymbol{E} \parallel c$ and $\boldsymbol{E} \perp c$ belong to Γ_4 and Γ_6 respectively, the orbital symmetries once again only allow the direct transition $\Gamma_1 \to \Gamma_4$ for $\boldsymbol{E} \parallel c$. Taking into account spin by going into the double group $\bar{D}_{3h}^1$, one finds from Table IV *b)* that the direct transition then takes place between Γ_7 and Γ_8. As expected the product $\Gamma_7 \times \Gamma_8 = \Gamma_3 + \Gamma_4 + \Gamma_6$ contains the representations of both $\boldsymbol{E} \parallel c$ and $\boldsymbol{E} \perp c$. Again the transition with $\boldsymbol{E} \perp c$ is possible only if spin and orbit are coupled and again this coupling gives rise to a mixing of the highest valence band Γ_7 with the lower-lying band Γ_7 originating from the band Γ_6^- of the β-modification.

4. – The direct-gap excitons in GaSe.

4·1. *The effective-mass approximation.* – Except for an investigation of the influence of exchange on the fine structure of exciton spectra the present dis-

cussion is based on the effective-mass approximation ([40,41]). In this approximation the wave functions of an exciton are of the form

$$\Psi_{ex}(\boldsymbol{K}, \boldsymbol{r}_e, \boldsymbol{r}_h) = \sum_{\boldsymbol{k}_h} F(\boldsymbol{k}_h, \boldsymbol{K})\, \psi_v(\boldsymbol{k}_h, \boldsymbol{r}_h)\, \psi_c(\boldsymbol{k}_h + \boldsymbol{K}, \boldsymbol{r}_e)\,, \tag{1}$$

where ψ_v and ψ_c are Bloch functions of valence and conduction bands and where the wave vector $\boldsymbol{K} = \boldsymbol{k}_e - \boldsymbol{k}_h$ is defined because of the translational invariance of the exciton Hamiltonian. The indices e and h relate to electrons and holes respectively. In an external magnetic field $\boldsymbol{H}$ whose vector potential can be chosen as

$$\boldsymbol{A}(\boldsymbol{r}) = \tfrac{1}{2}(\boldsymbol{H} \times \boldsymbol{r}) \tag{2}$$

the Fourier transform $F(\boldsymbol{r}_e, \boldsymbol{r}_h)$ of the envelope function $F(\boldsymbol{k}_h, \boldsymbol{K})$ is determined by the effective Schrödinger equation

$$\left[\frac{1}{2m_e^*}\left(\boldsymbol{p}_e + \frac{e}{c}\boldsymbol{A}(\boldsymbol{r}_e)\right)^2 + \frac{1}{2m_h^*}\left(\boldsymbol{p}_h - \frac{e}{c}\boldsymbol{A}(\boldsymbol{r}_h)\right)^2 - \frac{e^2}{\varepsilon|\boldsymbol{r}_e - \boldsymbol{r}_h|}\right] F(\boldsymbol{r}_e, \boldsymbol{r}_h) = \tag{3}$$

$$= E'_{ex} F(\boldsymbol{r}_e, \boldsymbol{r}_h)\,,$$

where $\boldsymbol{p}$ stands for the operator $-i\hbar\nabla$, m^* is an effective mass, ε an appropriate dielectric constant and where the exciton energy E'_{ex} is measured from the edge of the conduction band. Introducing centre-of-mass co-ordinates

$$\boldsymbol{R} = \frac{m_e^* \boldsymbol{r}_e + m_h^* \boldsymbol{r}_h}{m_e^* + m_h^*}\,, \qquad \boldsymbol{r} = \boldsymbol{r}_e - \boldsymbol{r}_h\,, \tag{4}$$

and performing the transformation

$$F(\boldsymbol{r}_e, \boldsymbol{r}_h) = \exp\left[i\left[\boldsymbol{K} - \frac{e}{\hbar c}\boldsymbol{A}(\boldsymbol{r})\right]\cdot\boldsymbol{R}\right] \Phi(\boldsymbol{r})\,, \tag{5}$$

we obtain the usual equation governing the internal motion of the exciton

$$\left[\frac{p^2}{2\mu} - \frac{e^2}{\varepsilon|\boldsymbol{r}|} + \frac{e}{\mu' c}\boldsymbol{A}\cdot\boldsymbol{p} + \frac{e^2}{2\mu c^2}A^2 - \frac{2e\hbar}{Mc}\boldsymbol{K}\cdot\boldsymbol{A}\right] \Phi(\boldsymbol{r}) = \tag{6}$$

$$= \left[E'_{ex} - \frac{\hbar^2 K^2}{2M}\right] \Phi(\boldsymbol{r}) = E_{ex}\Phi(\boldsymbol{r})\,.$$

([40]) R. S. KNOX: *Solid State Physics, Suppl.* **5** (New York, 1963).
([41]) J. O. DIMMOCK: *Semiconductors and Semimetals*, Vol. **3** (New York, 1967), p. 259.

Here the following abbreviations have been introduced:

$$(7)\qquad \begin{cases} \dfrac{1}{\mu} = \dfrac{1}{m_e^*} + \dfrac{1}{m_h^*}, \\ \dfrac{1}{\mu'} = \dfrac{1}{m_e^*} - \dfrac{1}{m_h^*} \\ \text{and} \\ M = m_e^* + m_h^*. \end{cases}$$

The different terms in (6) are:

the kinetic-energy operator

$$H_1 = \frac{p^2}{2\mu},$$

the Coulomb interaction

$$H_2 = -\frac{e^2}{\varepsilon |\boldsymbol{r}|}$$

between electron and hole in a medium of dielectric constant ε,

the Zeeman term

$$H_3 = \frac{e}{\mu' c} \boldsymbol{A}\cdot\boldsymbol{p}$$

which with the angular-moment operator $\boldsymbol{L}$ may be written as

$$H_3 = \frac{e}{2\mu' c} \boldsymbol{H}\cdot\boldsymbol{L},$$

the diamagnetic term

$$H_4 = \frac{e^2}{2\mu c^2} A^2,$$

the kinetic energy

$$H_5 = \frac{\hbar^2 K^2}{2M}$$

corresponding to the motion of the centre-of-mass and

the term

$$H_6 = -\frac{2e\hbar}{Mc} \boldsymbol{K}\cdot\boldsymbol{A} = -\frac{e\hbar}{Mc} [\boldsymbol{K}\cdot(\boldsymbol{H}\times\boldsymbol{r})]$$

which expresses the fact that the magnetic field couples the internal motion of the exciton to its centre-of-mass motion. Because its effect is equivalent to that of an electric field perpendicular to $\boldsymbol{H}$ and $\boldsymbol{K}$ it is sometimes referred to as the magneto-Stark term [42].

In order to account for the uniaxial symmetry of GaSe, we introduce anisotropic effective masses and dielectric constants whose components parallel and perpendicular to the c-axis of the crystal are

$$\begin{cases} m_{\parallel}^{*} = m_{z}^{*}, & \varepsilon_{\parallel} = \varepsilon_{z}, \\ m_{\perp}^{*} = m_{x}^{*} = m_{y}^{*}, & \varepsilon_{\perp} = \varepsilon_{x} = \varepsilon_{y}. \end{cases} \tag{8}$$

With (8) the terms H_i in eq. (6) become

$$\begin{aligned} H_1 &= \frac{1}{2\mu_x}(p_x^2 + p_y^2) + \frac{1}{2\mu_z} p_z^2, \\ H_2 &= -\frac{e^2}{\sqrt{\varepsilon_x \varepsilon_z}} \cdot \frac{1}{\sqrt{x^2 + y^2 + (\varepsilon_x/\varepsilon_z) z^2}}, \\ H_3 &= \frac{e}{\mu_x' c}(A_x p_x + A_y p_y) + \frac{e}{\mu_z' c} A_z p_z, \\ H_4 &= \frac{e^2}{2\mu_x c}(A_x^2 + A_y^2) + \frac{e^2}{2\mu_z c} A_z^2, \\ H_5 &= \frac{\hbar^2}{2M_x}(K_x^2 + K_z^2) + \frac{\hbar^2}{2M_z} K_z^2 \end{aligned} \tag{9}$$

and

$$H_6 = -\frac{2e\hbar}{M_x c}(K_x A_x + K_y A_y) - \frac{2e\hbar}{M_z c} K_z A_z .$$

This series of terms has to be completed by the addition to the Hamiltonian of a spin contribution, which we choose to be of the form

$$H_7 = \frac{e\hbar}{4mc}(g_x S_x H_x + g_y S_y H_y + g_z S_z H_z) . \tag{10}$$

$g_x = g_y = g_{\perp}$ and $g_z = g_{\parallel}$ are the components of the *exciton* g-factor and S_x, S_y and S_z those of the *total* exciton spin. In discussing the low-field magneto-optical properties of the excitons in GaSe, we will consider the terms H_3 to H_7 as perturbations.

---

[42] D. G. THOMAS and J. J. HOPFIELD: *Phys. Rev.*, **124**, 657 (1961).

The choice (10) of the spin Hamiltonian is justified since, as shown above, spin-orbit coupling is possible only via interband mixing and therefore is weak compared to exchange interaction (see below) which gives rise to appreciable spin-spin coupling.

4·2. *Field-free case*: $\boldsymbol{H} = 0$.

4·2.1. The anisotropic exciton. By introducing new co-ordinates

$$\boldsymbol{\rho} = \left(x, y, \sqrt{\frac{\mu_x}{\mu_z}}z\right) = (\xi, \eta, \zeta) \tag{11}$$

and neglecting the centre-of-mass motion, the field-free Schrödinger equation takes the form [18,19]

$$\left[\frac{1}{2\mu_x}(p_\xi^2 + p_\eta^2 + p_\zeta^2) - \frac{e^2}{\sqrt{\varepsilon_x \varepsilon_z}} \cdot \frac{1}{\sqrt{\xi^2 + \eta^2 + \zeta^2}} + P(\alpha)\right] \Phi(\boldsymbol{\rho}) = E_{\mathrm{ex}} \Phi(\boldsymbol{\rho}), \tag{12}$$

and one recognizes that the anisotropy now only appears in the perturbation term

$$P(\alpha) = \frac{e^2}{\sqrt{\varepsilon_x \varepsilon_z}}\left[\frac{1}{\sqrt{\xi^2 + \eta^2 + \zeta^2}} - \frac{1}{\sqrt{\xi^2 + \eta^2 + \alpha\zeta^2}}\right], \tag{13}$$

which belongs to the group $D_{\infty h}$. The anisotropy parameter α is defined by

$$\alpha = \frac{\mu_x \varepsilon_x}{\mu_z \varepsilon_z}. \tag{14}$$

The zeroth-order solutions of (12) are the hydrogenic functions which correspond to the eigenvalues

$$E_{0\mathrm{ex}}^{(n)} = -\frac{\mu_x}{2\varepsilon_x \varepsilon_z} \cdot \frac{e^4}{\hbar^2} \cdot \frac{1}{n^2} = -\frac{R}{n^2} \cdot \frac{\mu_x}{m} \cdot \frac{1}{\varepsilon_x \varepsilon_z} \tag{15}$$

and are localized within the radii

$$a_{0\mathrm{ex}}^{(n)} = \frac{\hbar^2}{\mu_x e^2} \sqrt{\varepsilon_x \varepsilon_z}\, n^2 = a_{\mathrm{B}} \cdot n^2 \cdot \frac{m}{\mu_x} \sqrt{\varepsilon_x \varepsilon_z}. \tag{16}$$

Here R stands for the Rydberg constant and a_{B} is the first Bohr radius of the hydrogen atom. In spite of the anisotropy it is possible, therefore, to classify the exciton states in terms of the quantum numbers n, l and m of the hydrogen levels. However, the perturbation $P(\alpha)$ does not only remove some of the accidental degeneracies of these levels, but it also mixes some of them.

Thus DÉVERIN ([21,22]), who has discussed eq. (12) in detail, has shown that beginning with $n = 3$ the s and d_0 levels belonging to the same n show appreciable mixing. Déverin's findings concerning the dependence of the s and p levels on the anisotropy parameter α are represented in Fig. 6. It follows from this Figure that, if in addition to an s level at least one of the p levels of the same principal quantum number can be observed, then α can be determined. We will see below that for $\boldsymbol{H} = 0$ only the exciton s states are visible. However, in the Voigt geometry the magneto-Stark term mixes some s character into the

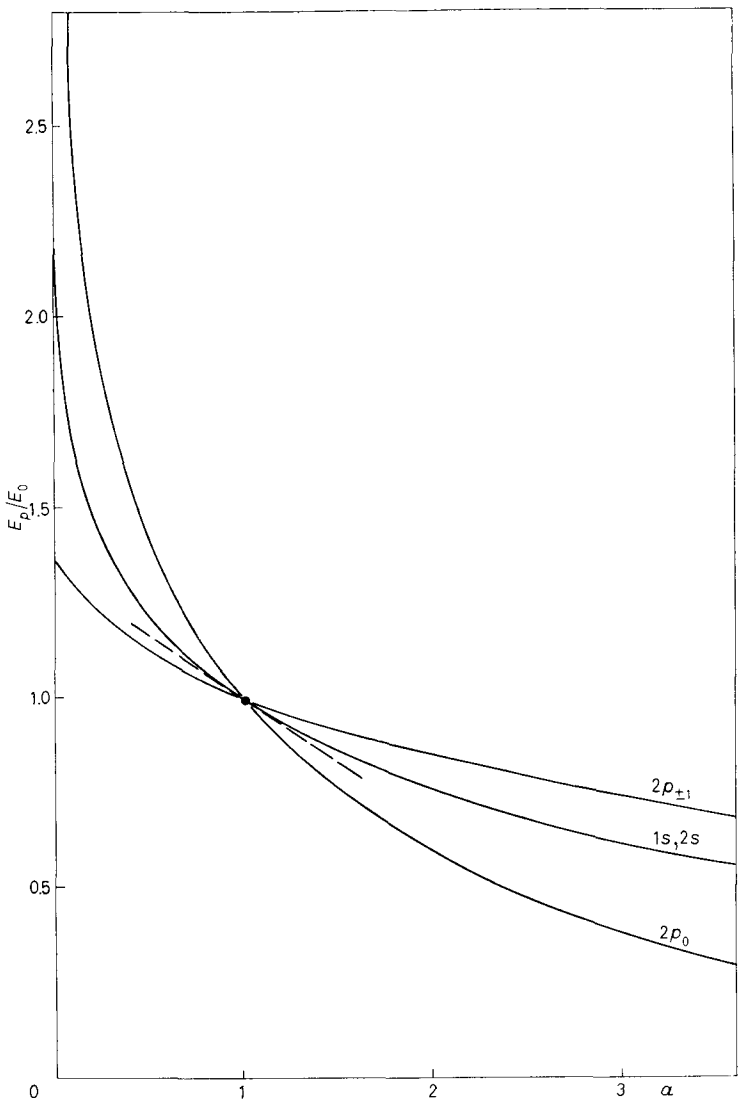

Fig. 6. – The dependence on the anisotropy parameter α of the s and p exciton states (after DÉVERIN ([21])). $\alpha = \mu_x \varepsilon_x / \mu_z \varepsilon_z$.

p_y states which thus become visible as $\boldsymbol{H}$ increases. It is therefore possible by extrapolation to determine the position of p_y for $\boldsymbol{H} = 0$ and hence to obtain an experimental value for α.

4·2.2. Spin-orbit coupling. We have seen in Sect. 3 that the direct transition at the fundamental edge takes place between the valence and conduction band spinors belonging to the representations Γ_7 and Γ_8 of the group $\bar{D}^1_{3h}$ of the single layer. Since the s envelopes $\Phi_s(\boldsymbol{\rho})$ transform according to Γ_1 of this group, the following four s-like exciton states are possible in GaSe:

$$\Gamma^{(s)}_{ex} = \Gamma_7 \times \Gamma_8 \times \Gamma_1 = \Gamma_4 + \Gamma_3 + \Gamma_6 . \tag{17}$$

If exchange effects are neglected, they are all degenerate because spin-orbit coupling does not split valence and conduction bands. However, as mentioned earlier, spin-orbit coupling mixes two valence bands and because the mixing bands are separated by an estimated 500 meV the coupling is weak. It is reasonable, therefore, to analyse the exciton states (17) in terms of eigenstates of defined spin multiplicity. To do so we construct the exciton s functions from the Bloch orbits Γ_1 and Γ_4 of D^1_{3h} and from the two-particle spin functions

$$\left.\begin{aligned} \chi(S, S_z) = \chi(0, \quad 0) &= \frac{1}{\sqrt{2}} (\alpha_e \beta_h - \alpha_h \beta_e) , \quad D^{(0)}, \\ \chi(1, \quad 0) &= \frac{1}{\sqrt{2}} (\alpha_e \beta_h + \alpha_h \beta_e) , \\ \chi(1, +1) &= \alpha_e \alpha_h , \\ \chi(1, -1) &= \beta_e \beta_h , \end{aligned}\right\} D^{(1)}, \tag{18}$$

which transform like $D^{(0)} = \Gamma_1$ and $D^{(1)} = \Gamma_2 + \Gamma_5$ respectively. The resulting singlet s exciton has the symmetry

$$\Gamma^{(s)}_{sing} = \Gamma_1 \times \Gamma_4 \times \Gamma_1 \times D^{(0)} = \Gamma_4 , \tag{19}$$

while the triplet s excitons have the symmetries

$$\Gamma^{(s)}_{trip} = \Gamma_1 \times \Gamma_4 \times \Gamma_1 \times D^{(1)} = \Gamma_3 + \Gamma_6 . \tag{20}$$

Since these states have no common representations there is no first-order singlet-triplet mixing and to within this approximation the four exciton states (17) have pure singlet and pure triplet character respectively. The polarization vector $\boldsymbol{E} \parallel c$ belongs to the representation Γ_4 of D^1_{3h}. The singlet can therefore be observed in light polarized along c. Transitions into the triplet states, however, involve a change of the spin of the excited electron and since the dipole operator does not operate on spin the oscillator strength of the triplet states is zero in spite of the fact that $\boldsymbol{E} \perp c$ belongs to Γ_6.

In order to account for the experimental fact that the Γ_6 states can be observed in absorption, one has to go beyond the present two-band model and consider interband mixing resulting from spin-orbit coupling. In discussing the band-to-band transition at Γ we have seen that the mixing occurs between the valence bands Γ_4^- and Γ_6^- of D_{6h}^4, which become Γ_1 and Γ_5 in D_{3h}^1 and finally Γ_7 and $\Gamma_7+\Gamma_9$ in $\bar{D}_{3h}^1$. If once again we analyse the exciton states in terms of eigenfunctions of definite multiplicity and if by $[\Gamma_1+\gamma\Gamma_5]$ we symbolically describe the mixed character of the valence band, we find for the singlet

$$[\Gamma_1+\gamma\Gamma_5]\times\Gamma_4\times\Gamma_1\times D^{(0)}=\Gamma_4+\gamma\Gamma_6 \tag{21}$$

and for the triplet

$$[\Gamma_1+\gamma\Gamma_5]\times\Gamma_4\times\Gamma_1\times D^{(1)}=\Gamma_3+\Gamma_6+\gamma[\Gamma_3+\Gamma_4+\Gamma_5+\Gamma_6]\,. \tag{22}$$

Obviously the singet and triplet states now mix and the four band edge excitons (17) become

$$\begin{cases} \Gamma_4=|\text{singlet}\rangle+\dfrac{C}{\Delta E_{\Gamma_4}}|\text{triplet}\rangle\,, \\ \Gamma_3=|\text{triplet}\rangle\,, \\ \Gamma_6=|\text{triplet}\rangle+\dfrac{C}{\Delta E_{\Gamma_6}}|\text{singlet}\rangle\,. \end{cases} \tag{23}$$

The value of C is determined by the strength of the spin-orbit coupling and in turn determines the oscillator strengths of the Γ_4 and Γ_6 excitons which now are finite. The energies $\Delta E_{\Gamma_4}\approx\Delta E_{\Gamma_6}$ are of the order of the valence band separation $\Delta E\approx 500$ meV.

4·2.3. Selection rules. The group-theoretical considerations on which the above discussion of the spin-orbit coupling is based are summarized in Tables V and VI. These Tables contain the selection rules for the creation of *s*-, *p*- and *d*-like excitons by the absorption of light polarized parallel and perpendicular to the crystal *c*-axis. Table V relates to spin-orbit coupling weak enough that the band mixing resulting from this coupling can be neglected (*LS* coupling limit). Table VI relates to strong spin-orbit coupling (*JJ* coupling limit).

The selection rules state that an exciton can only be created by the absorption of a photon:

if the probability of finding electron and hole in the same position is nonzero, *i.e.* if $|\Phi(0)|^2\neq 0$ (higher-order transitions resulting from $|\nabla\Phi(0)|^2\neq 0$ are neglected); and

if the representation of the exciton state contains the representation of the polarization vector of the photon which is to be absorbed.

TABLE V. – *Selection rules for the exciton in* GaSe: $\boldsymbol{H}=0$. Weak spin-orbit coupling (*LS* coupling limit). Group D_{3h}^1: $\boldsymbol{E}\parallel c$ belongs to Γ_4, $\boldsymbol{E}\perp c$ to Γ_6.

1	2	3	4	5	6	7	8	9	10	11	12	13
Bloch functions $\psi(\boldsymbol{k}, \boldsymbol{r})$	$\psi_v \cdot \psi_c$	Envelope Φ_{nlm}	Orbit $\psi_v \cdot \psi_c \cdot \Phi_{nlm}$	Spin $\chi(\boldsymbol{S}, S_z)$	Exciton $\psi_v \cdot \psi_c \cdot \Phi \cdot \chi$	Visible for	$\lvert\Phi\rvert^2 \neq 0$	Orbit alone	Orbit plus spin	Mixing with s	Strength of absorption	Multiplet component
ψ_v: Γ_1 ψ_c: Γ_4	Γ_4	s, d_0: Γ_1	Γ_4	$\chi(0, 0)$: Γ_1	Γ_4	$\boldsymbol{E}\parallel c$	+	+	+		strong	singlet
				$\chi(1, 0)$: Γ_2	Γ_3							
				$\chi(1, \pm 1)$: Γ_5	Γ_6	$\boldsymbol{E}\perp c$	+		+		weak	triplet
		p_0: Γ_4	Γ_1		Γ_1							
					Γ_2							
					Γ_5							
		$p_{\pm 1}, d_{\pm 2}$: Γ_6	Γ_5		Γ_5							
					Γ_5							
					$\Gamma_1+\Gamma_2+\Gamma_6$	$\boldsymbol{E}\perp c$				+	very weak	triplet
		$d_{\pm 1}$: Γ_5	Γ_6		Γ_6	$\boldsymbol{E}\perp c$				+	very weak	singlet
					Γ_6	$\boldsymbol{E}\perp c$				+	very weak	triplet
					$\Gamma_3+\Gamma_4+\Gamma_5$	$\boldsymbol{E}\parallel c$				+	very weak	triplet

TABLE VI. – *Selection rules for the excitons in* GaSe: $\boldsymbol{H}=0$. Strong spin-orbit coupling (JJ coupling limit). Double group $\bar{D}^1_{3h}$: $\boldsymbol{E}\parallel c$ belongs to Γ_4, $\boldsymbol{E}\perp c$ to Γ_6.

1	2	3	4	5	6	7	8
Band spinors $\psi(\boldsymbol{k}, \boldsymbol{r}, \sigma)$	$\psi_v\cdot\psi_c$: $\Gamma_3+\Gamma_4+\Gamma_6$	Envelope Φ_{nlm}	Exciton $\psi_v\cdot\psi_c\Phi_{nlm}$	Visible for	$\lvert\Phi(0)\rvert^2\neq 0$	Mixing with s	Strength of absorption
ψ_v: Γ_7 ψ_c: Γ_8	Γ_3	s, d_0: Γ_1	Γ_3				
		p_0: Γ_4	Γ_2				
		$p_{\pm1}, d_{\pm2}$: Γ_6	Γ_5				
		$d_{\pm1}$: Γ_5	Γ_6	$\boldsymbol{E}\perp c$		+	weak
	Γ_4		Γ_4	$\boldsymbol{E}\parallel c$	+		strong
			Γ_1				
			Γ_5				
			Γ_6	$\boldsymbol{E}\perp c$		+	weak
	Γ_6		Γ_6	$\boldsymbol{E}\perp c$	+		strong
			Γ_5				
			$\Gamma_1+\Gamma_2+\Gamma_6$	$\boldsymbol{E}\perp c$		+	weak
			$\Gamma_3+\Gamma_4+\Gamma_5$	$\boldsymbol{E}\parallel c$		+	weak

The first of these conditions signifies that only s-like states and states which mix with them are visible in absorption. The mixing occurs on different levels. Thus s- and d_0-like states mix via the perturbation operator $P(\alpha)$. The « mixing with s » marked in Tables V and VI, however, is possible only because of the total exciton symmetry in the groups D^1_{3h} and $\bar{D}^1_{3h}$.

In column 12 of Table V an estimate is made of the expected strength of absorption of the different exciton states in the case of weak spin-orbit coupling. This estimate is based on the following considerations:

With its total symmetry (column 6) containing the representation of one of the polarization vectors an exciton state gives rise to a strong absorption if $|\Phi(0)|^2 \neq 0$ *and* if its orbital symmetry alone (colum 4) already is of the proper symmetry. If only spin and orbit together have the right symmetry, then its absorption is weak, because it results from the weak spin-orbit coupling induced band mixing.

If for a given state $|\Phi(0)|^2 = 0$ and if its orbital symmetry allows for « mixing with s » (column 11), then the absorption due to this state can at best be as strong as that of the s-like state with which it mixes. If only orbit plus spin allow for mixing, the absorption will be much weaker than that of the s-like state.

A similar estimate for the case of strong spin-orbit coupling is given in column 8 of Table VI:

If the symmetry of a state contains the representation of $\boldsymbol{E} \parallel c$ or $\boldsymbol{E} \perp c$, its absorption is strong or weak depending on whether the state is s-like or mixes with such a state.

4'2.4. Fine structure of the ground state. The ground state of the exciton series observed in absorption and reflexion in samples of γ- and ε-GaSe show a marked fine structure (see Fig. 9 below). Part of this structure can be ascribed to the existence in these samples of glide stacking faults which intimately mix the two modifications and thus give rise to statistical stacking sequences (see Sect. **2**).

In the present treatment of the exciton the screening of the Coulomb interaction between electron and hole is described by a dielectric tensor ε_γ. However, since the exciton extends over a finite volume only the ε_γ which according to eq. (15) determines the exciton energy depends somewhat on the actual stacking configuration A_N of the N layers embraced by the exciton:

$$\varepsilon_\gamma = \varepsilon_\gamma(A_N)\,. \tag{24}$$

The number s_N of nonequivalent stacking configurations of N layers is

$$s_N = \left\{ \begin{array}{ll} 2^{N-2} & \text{for even } N \\ 2^{N-2} + 2^{(N-3)/2} & \text{for odd } N \end{array} \right\} \approx 2^{N-2} \qquad \text{for large } N\,. \tag{25}$$

Because of (24) a slightly different exciton energy $E_{ex}^{(n)}(A_N)$ corresponds to each of them. If all s_N sequences A_N are realized, an exciton state of principal quantum number n therefore gives rise to a series of s_N energetically different absorption lines: it exhibits a fine structure.

N is proportional to the exciton radius and hence to n^2. The number of fine-structure components of a state therefore increases with the quantum number n like 2^{n^2}. However, the energetic separation between them is proportional to the exciton energy $E_{ex}^{(n)}$, *i.e.* to $1/n^2$, and it is therefore understandable why the fine structure can only be resolved in the ground state $n = 1$. The maximum number of ground-state components which can be attributed to stacking faults was found to be about ten ([25]). According to (25) the value $s_N = 10$ corresponds to $N = 5$, *i.e.* the ground-state of the exciton in GaSe extends over 5 layers and its fine-structure components belong to the stacking configurations A_5.

It should be noted that, if a crystal is very badly deformed, individual layers may tear and structural defects other than glide stacking faults will begin to influence the exciton spectrum. In this situation the fine structure of the ground state is smeared out, resulting in a broad featureless line and the excited states are no longer visible at all.

Exchange interaction gives rise to an additional fine structure of the exciton states. Indeed, since the band mixing induced by spin-orbit coupling is relatively weak (Subsect. **4**·2.2), the multiplet character of the exciton states is well preserved. Moreover, since only singlet states or states with an appreciable admixture of singlet character ([40,41]) contain an exchange term, singlet and triplet states are energetically separated. The fine-structure components associated with stacking faults therefore are multiplied, appearing once for each multiplet component.

The operator which describes the exchange interaction and which has to be added to the effective-mass Hamiltonian (9) can be written in the form ([43])

$$H_s = J(\boldsymbol{K})\,\delta_M \delta(\boldsymbol{r})\,, \tag{26}$$

where the symbols δ_M and $\delta(\boldsymbol{r})$ indicate that H_s is nonzero only for s-like singlet states.

H_s may be split into two terms:

the short-range exchange J_1 is independent of $\boldsymbol{K}$ and may be written in terms of valence and conduction band Wannier functions a_v and a_c centred at the origin:

$$J_1 \approx 2\,\langle a_c(\boldsymbol{r}_1)\,a_v(\boldsymbol{r}_2)|\,\frac{e^2}{r_{1,2}}\,|a_v(\boldsymbol{r}_1)\,a_c(\boldsymbol{r}_2)\rangle\,; \tag{27}$$

([43]) Y. ONODERA and Y. TOYOZAWA: *Journ. Phys. Soc. Japan*, **22**, 833 (1967).

the long-range exchange $J_2(\boldsymbol{K})$ has to be evaluated from a sum over all lattice vectors $\boldsymbol{T}$:

$$J_2(\boldsymbol{K}) \approx 2 \sum_{\boldsymbol{T}\neq 0} \exp[i\boldsymbol{K}\cdot\boldsymbol{T}] \langle a_c(\boldsymbol{r}_1 - \boldsymbol{T}) a_v(\boldsymbol{r}_2) | \frac{e^2}{r_{1,2}} | a_v(\boldsymbol{r}_1 - \boldsymbol{T}) a_c(\boldsymbol{r}_2)\rangle \,. \tag{28}$$

It is nonzero whenever the transition densities have nonzero dipole moments

$$\boldsymbol{d} = \langle a_v(\boldsymbol{r}) | \boldsymbol{r} | a_c(\boldsymbol{r})\rangle \neq 0 \,, \tag{29}$$

its actual value depending on the relative orientation of $\boldsymbol{d}$ and $\boldsymbol{K}$. The $\boldsymbol{K}$-dependence of J_2 gives rise to a spatial dispersion, *i.e.* to the so-called longitudinal-transversal shift ([40]) of the singlet exciton states.

A detailed discussion of the influence of exchange upon the exciton states in GaSe is given elsewhere ([44]).

It follows from (26) that the exchange energy $\langle \Phi_{nlm} | H_8 | \Phi_{nlm}\rangle$ is proportional to $|\Phi_{nlm}(0)|^2$ decreasing like $1/n^3$ with increasing n. The exchange splitting is therefore appreciable only in the ground state.

Summing up the findings of this Section, we write down the energies $E^{(1s)}_{\Gamma_4}(A_5)$ and $E^{(1s)}_{\Gamma_6}(A_5)$ of the fine-structure components of the singlet (Γ_4) and of two of the triplet (Γ_6) ground states

$$E^{(1s)}_{\Gamma_4}(A_5) = E^{(1s)}_{ex}(A_5) + \langle \Phi_{1s} | H_8 | \Phi_{1s}\rangle - \frac{C^2}{\Delta E_{\Gamma_4}} \,, \tag{30}$$

$$E^{1s}_{\Gamma_6}(A_5) = E^{(1s)}_{ex}(A_5) - \frac{C^2}{\Delta E_{\Gamma_6}} \,, \tag{31}$$

where the last terms have been added to account for the mixing of the valence bands caused by the spin-orbit coupling (see eq. (23)). Since experiment shows that the multiplet character of the exciton states is clearly recognizable in spite of the spin-orbit coupling we have $C \ll \Delta E_{\Gamma_4} \approx \Delta E_{\Gamma_6}$. The difference $\Delta E_{\Gamma_4,\Gamma_6}(A_5)$ between the $1s$ singlet and triplet components belonging to the same stacking sequence A_5 therefore is essentially equal to the total exchange energy. It should be noted that regardless of its smallness C cannot be neglected because it is responsible for the nonzero oscillator strength of the Γ_6 states (see Subsect. 4·2.2).

4·3. *The exciton in a magnetic field.* – Allowance being made for a spin contribution, the influence of a magnetic field $\boldsymbol{H}$ upon the exciton energies is studied within the effective-mass approximation only. Contributions induced by the symmetry of the Bloch functions of valence and conduction bands are neglected since the corresponding energies are small, *i.e.* of the order of the

([44]) F. BASSANI and M. SCHLÜTER: in preparation.

ratio $\Omega_{u.c.}/\Omega_{ex} \approx 10^{-2}$ between the unit cell and the exciton volumes. Moreover, although the selection rules for optical transitions are derived for the full crystal symmetry with the magnetic field applied, an optical transition to an exciton state is considered as allowed only if it is allowed in the effective-mass approximation: transitions which are allowed beyond this approximation because of the symmetry of the crystal field have probabilities which are smaller by a factor $(\Omega_{u.c.}/\Omega_{ex})^2 \approx 10^{-4}$.

Throughout this paper the magnetic field is considered as a perturbation. Its contributions to the energy of an exciton state therefore are obtained from the matrix elements $\langle \Phi_{nlm}|H_i'|\Phi_{n'l'm'}\rangle$ evaluated between the zeroth-order solutions Φ_{nlm} of eq. (12). Note that the operator carries a prime to indicate that it is written in the co-ordinates $\boldsymbol{\rho} = (x, y, \sqrt{\mu_x/\mu_z}z)$.

The perturbation treatment proposed here is limited to fields for which all the elements $\langle \Phi|H_i|\Phi\rangle$, $i = 3, 4, 6$, remain small compared to the ionization energies of the corresponding field-free state Φ. In practice this means that we are able only to consider states with $n \leqslant 2$. The high-field case has been treated in ref. [8-12] and the difficult problem of connecting the field-free exciton level with the high-field Landau levels was discussed in ref. [14,15].

4·3.1. The Faraday geometry. The Faraday geometry is characterized by the fact that the light, whose interaction with the crystal is to be

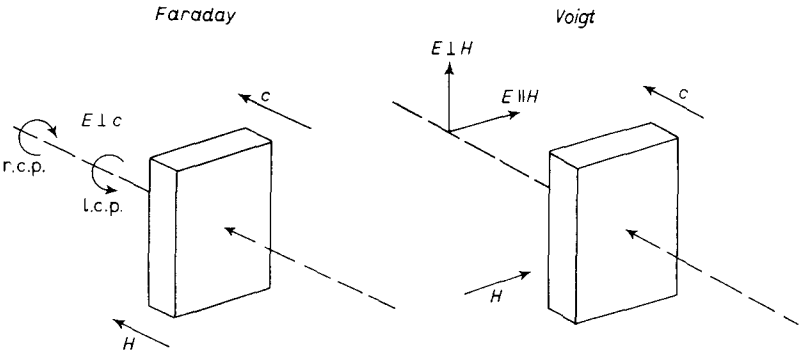

Fig. 7. – The geometries of the magneto-absorption measurements.

studied, is parallel to the applied magnetic field (see Fig. 7). In view of our experiment we consider the case

$$\boldsymbol{H} = (0, 0, H_z), \tag{32}$$

and, since the exciton takes over momentum from photons running along z, we have

$$\boldsymbol{K} = (0, 0, K_z). \tag{33}$$

According to (9) the corresponding vector potential

$$A = \left(-\frac{y}{2} H_z, \frac{x}{2} H_z, 0\right) \tag{34}$$

then gives rise to the Zeeman term

$$H_3 = H_3' = \frac{ie\hbar}{2\mu_x' c} \cdot H_z \left\{ y \frac{\partial}{\partial x} - x \frac{\partial}{\partial y} \right\} = \frac{e}{2\mu_x' c} H_z L_z , \tag{35}$$

where

$$L_z = \frac{\hbar}{i} \left(x \frac{\partial}{\partial y} - y \frac{\partial}{\partial x} \right)$$

is the operator of the z-component of angular momentum.

The diamagnetic term is

$$H_4 = H_4' = \frac{e^2}{8\mu_x c^2} H_z^2 (x^2 + y^2) . \tag{36}$$

Because of (32) the magneto-Stark term H_6 is zero.

In the effective-mass approximation H_3' and H_4' have only diagonal matrix elements in the basis set formed by the hydrogenic s, p_0, p_{+1} and p_{-1} functions. There is no s-p mixing and according to Table V the $p_{\pm 1}$ levels will therefore at best be very weakly visible even in the presence of a magnetic field along z. In fact none of the p levels has been observed experimentally so that only s states need to be considered here and since H_3' does not operate on s functions one is finally left with the matrix elements

$$\begin{cases} \langle 1s|H_4'|1s\rangle = \sigma H_z^2 , \\ \text{and} \\ \langle 2s|H_4'|2s\rangle = 14\sigma H_z^2 , \end{cases} \tag{37}$$

where

$$\sigma = \frac{e^2}{4mc^2} \cdot a_B \cdot \frac{m^3}{\mu_x^3} \varepsilon_x \varepsilon_z = \frac{e^2}{4\mu_x c^2} (a_{0ex}^{(1)})^2 , \tag{38}$$

and where a_B and $a_{0ex}^{(1)}$ are defined in eq. (16).

With (32) the spin term (10) is

$$H_7 = \frac{e\hbar}{4mc} g_z S_z H_z , \tag{39}$$

where the spin component S_z takes the values zero for the singlet and one of the triplet states, and ± 1 for the remaining triplet states.

TABLE VII. – *Selection rules for the excitons in* GaSe: Faraday geometry $\boldsymbol{H} = (0, 0, H_z)$, $\boldsymbol{E} = (E_x, E_y, 0)$. Weak spin-orbit coupling (LS coupling limit). Group C_{3h}^1: l.c.p. light belongs to Γ_2, r.c.p. light to Γ_3.

$\psi(\boldsymbol{k}, \boldsymbol{r})$	$\psi_v \cdot \psi_c$	Φ_{nlm}	$\psi_v \cdot \psi_c \cdot \Phi$	$\chi(\boldsymbol{S}, S_z)$	$\psi_v \cdot \psi_c \cdot \Phi \cdot \chi$	Visible for	Strength of absorption	Multiplet component
ψ_v: Γ_1 ψ_c: Γ_4	Γ_4	s, d_0: Γ_1	Γ_4	$\chi(0, 0)$: Γ_1	Γ_4			singlet
				$\chi(1, 0)$: Γ_1	Γ_4			triplet
				$\chi(1, +1)$: Γ_5	Γ_2	l.c.p.	weak	triplet
				$\chi(1, -1)$: Γ_6	Γ_3	r.c.p.	weak	triplet

In Table VII the selection rules for excitons in the Faraday geometry are given. In view of our earlier findings we have only taken into account the LS coupling limit corresponding to weak spin-orbit coupling. Furthermore, since the magnetic field applied along z does not give rise to mixing of exciton states beyond the one already met in the field-free case, we only consider s states. The z-axis is parallel to the crystal c-axis. Light incident along this axis therefore has its polarization vector $\boldsymbol{E} \perp c$ and may be right (r.c.p.) and left (l.c.p.) circularly polarized.

4·3.2. The Voigt geometry. The Voigt geometry is characterized by the fact that the incident light and the applied magnetic field are perpendicular to one another (Fig. 7). The experiments were carried out in light running along z, whence once more

$$\boldsymbol{K} = (0, 0, K_z) , \tag{40}$$

and in a magnetic field along x

$$\boldsymbol{H} = (H_x, 0, 0) . \tag{41}$$

The corresponding vector potential is

$$\boldsymbol{A} = \left(0, -\frac{z}{2} H_x, \frac{y}{2} H_x\right) , \tag{42}$$

and gives rise to a linear Zeeman term which in the co-ordinates $(x, y, \sqrt{\mu_x/\mu_z}\, z)$ of the hydrogenic envelopes is

$$H_3' = \frac{ie\hbar}{2\mu_x' c} \cdot H_x \left(\frac{\mu_z}{\mu_x}\right)^{\frac{1}{2}} \cdot \left(\frac{\mu_x'}{\mu_z'} y \frac{\partial}{\partial z} - \frac{\mu_x}{\mu_z} z \frac{\partial}{\partial y}\right) = - \frac{e}{2\mu_x' c} H_x (b^+ L_x^- + b^- L_x^+) , \tag{43}$$

with

$$b^{\pm}=\frac{1}{2}\left(\frac{\mu_z}{\mu_x}\right)^{\frac{1}{2}}\left(\frac{\mu_x'}{\mu_z'}\pm\frac{\mu_z}{\mu_x}\right)$$

and

$$L_x^{\pm}=\frac{\hbar}{i}\left(y\frac{\partial}{\partial z}\pm z\frac{\partial}{\partial y}\right).$$

Since the contributions of the operator L_x^+ are off-diagonal in n ([22]) they may be neglected and H_3' takes the approximate form

$$H_3'\approx-\frac{e}{2\mu_x' c}\cdot b^+L_xH_x\,, \tag{44}$$

where $L_x=L_x^-$ is the operator of the x-component of angular momentum.

The diamagnetic term H_4' and the magneto-Stark term H_6' are respectively

$$H_4'=\frac{e^2}{8\mu_z c^2}\cdot H_x^2(y^2+z^2) \tag{45}$$

and

$$H_6=H_6'=\frac{e\hbar}{M_z c}H_xK_xy\,. \tag{46}$$

Since angular momentum is not conserved in the Voigt geometry, it is convenient to use s, p_x, p_y and p_z as basis set. The operator L_x and hence H_3' have no diagonal elements in this basis, but there is an off-diagonal element which mixes the p states whose axes are perpendicular to $\boldsymbol{H}$:

$$\langle 2p_y|H_3'|2p_z\rangle=\frac{ie\hbar}{2\mu_x' c}b^+H_x\,. \tag{47}$$

The diamagnetic term H_4' gives rise to the following diagonal elements:

$$\left|\begin{array}{l}\langle 1s|H_4'|1s\rangle=\sigma\dfrac{\mu_x}{\mu_z}H_x^2\,,\\[2ex] \langle 2s|H_4'|2s\rangle=14\sigma\dfrac{\mu_x}{\mu_z}H_x^2\,,\\[2ex] \langle 2p_x|H_4'|2p_x\rangle=6\sigma\dfrac{\mu_x}{\mu_z}H_x^2\\[2ex] \text{and}\\[2ex] \langle 2p_y|H_4'|2p_y\rangle=\langle 2p_z|H_4'|2p_z\rangle=12\sigma\dfrac{\mu_x}{\mu_z}H_x^2\,,\end{array}\right. \tag{48}$$

where once again

$$\sigma = \frac{e^2}{4\mu_x c^2} (a_{0\mathrm{ex}}^{(1)})^2 .$$

H_4' has no off-diagonal elements.

Comparing the first two equations of (48) with (37), one recognizes that from the experimentally determined diamagnetic shifts corresponding to the two geometries the reduced effective-mass ratio μ_x/μ_z can be evaluated.

As mentioned in Subsect. 4·1 the magneto-Stark effect is equivalent to the effect of an electric field applied perpendicular to $\boldsymbol{K}$ and $\boldsymbol{H}$. In the present geometry this field would run along the y-axis and would thus mix the s and p_y states. The magneto-Stark effect therefore gives rise to the off-diagonal term

$$\langle 2s|H_6'|2p_y\rangle = \frac{e\hbar}{2M_z c} \cdot a_{0\mathrm{ex}}^{(1)} H_x K_z , \tag{49}$$

which with $K_z = 2\pi n/\lambda$, where n is the index of refraction at the wavelength λ, and with an adequate value of M_z approaches the value of the linear Zeeman term. As mentioned in Subsect. 4·2.1 the H_6' induced s-p_y mixing is of considerable importance since it permits the relative positions of the s and p levels to be determined by extrapolation to $\boldsymbol{H}=0$. An experimental value for the anisotropy parameter α may thus be obtained.

Concerning the spin contributions to the exciton energy we note that the spin functions (18) which are quantized along z are mixed by the operator $S_x H_x$. In terms of the $\chi(\boldsymbol{S}, S_x)$ the new spin functions and their representations in the group C_s^1 are

$$\left\{\begin{array}{lll}
\chi_1 = \chi(0,0) , & \Gamma_1 , & \text{singlet} , \\
\chi_2 = \dfrac{1}{\sqrt{2}} [\chi(1,+1) - \chi(1,-1)] , & \Gamma_1 , & \text{triplet} , \\
\chi_3 = \dfrac{1}{\sqrt{2}} \left[\chi(1,0) + \dfrac{1}{\sqrt{2}} \chi(1,+1) + \dfrac{1}{\sqrt{2}} \chi(1,-1)\right] , & \Gamma_2 , & \text{triplet} , \\
\chi_4 = \dfrac{1}{\sqrt{2}} \left[\chi(1,0) - \dfrac{1}{\sqrt{2}} \chi(1,+1) - \dfrac{1}{\sqrt{2}} \chi(1,-1)\right] , & \Gamma_2 , & \text{triplet} .
\end{array}\right. \tag{50}$$

The corresponding eigenvalues of the operator H_7 are

$$\left\{\begin{array}{l}
\langle \chi_1|H_7|\chi_1\rangle = \langle \chi_2|H_7|\chi_2\rangle = 0 , \\
\langle \chi_3|H_7|\chi_3\rangle = +\dfrac{e\hbar}{4mc} g_x H_x , \\
\langle \chi_4|H_7|\chi_4\rangle = -\dfrac{e\hbar}{3mc} g_x H_x .
\end{array}\right. \tag{51}$$

We are now in a position to write down the energies of the excitons as functions of the magnetic field in the Voigt geometry. Leaving away the terms giving rise to a fine structure, we find for $n=1$

$$(52)\qquad \left|\begin{array}{l} E_{\Gamma_1}^{(1s)} = E_{ex}^{(1s)} + \sigma\frac{\mu_x}{\mu_z}H_x^2 \\ \text{and} \\ E_{\Gamma_2}^{(1s)} = E_{ex}^{(1s)} + \sigma\frac{\mu_x}{\mu_z}H_x^2 \pm \frac{e\hbar}{4mc}g_x H_x\,. \end{array}\right.$$

The situation is more complicated in the case $n=2$ which calls for the diagonalization of the 4×4 matrix involving the $2s$ and $2p$ states. Since in the s, p_x, p_y, p_z basis and in the effective-mass approximation a magnetic field along x does not mix p_x with any of the other states, the matrix decomposes into a 1×1 block and a 3×3 block and one has

$$(53)\qquad \left|\begin{array}{l} E_{\Gamma_2}^{(2p_x)} = E_{ex}^{(2p_{\pm1})} + 6\sigma\frac{\mu_x}{\mu_z}H_x^2 \\ \text{and} \\ E_{\Gamma_1}^{(2p_x)} = E_{ex}^{(2p_{\pm1})} + 6\sigma\frac{\mu_x}{\mu_z}H_x^2 \pm \frac{e\hbar}{4mc}g_x H_x\,. \end{array}\right.$$

The symmetries of these states are Γ_2 and Γ_1 respectively but since the states are pure p they are not visible experimentally.

The 3×3 matrix from which the energies and the percentages of s-character of the mixed states can be computed is

(54)

	s	p_y	p_z
s	$E_{ex}^{(2s)} + 14\alpha_D H_x^2$	$\alpha_{MS}H_x$	0
p_y	$\alpha_{MS}H_x$	$E_{ex}^{(2p_{\pm1})} + 12\alpha_D H_x^2$	$\alpha_L H_x$
p_z	0	$\alpha_L^* H_x$	$E_{ex}^{(2p_0)} + 12\alpha_D H_x^2$

where

$$\alpha_D = \sigma\frac{\mu_x}{\mu_z}, \qquad \alpha_L = -\frac{ie\hbar}{2\mu_x' c}\cdot b^+ \qquad \text{and} \qquad \alpha_{MS} = \frac{e\hbar}{2M_z c}\,a_{0ex}^{(1)}K_z\,.$$

Since the oscillator strength of a state is proportional to the square of its percentage of s-character and since there is no first-order s-p_z mixing, only the states which correlate with the field-free s and p_y states are visible in the experiment. The computed energies and oscillator forces of the mixed states adjusted to fit the experimental data are shown in Fig. 14 as functions of H_x. The values of α_D, α_L and α_{MS} derived from this fit are given in Subsect. 5·3.2 below.

TABLE VIII. – *Selection rules for the excitons in* GaSe: Voigt geometry $\boldsymbol{H}=(H_x, 0, 0)$, $\boldsymbol{E}=(E_x, E_y, 0)$. Weak spin-orbit coupling (LS coupling limit). Group C_s^1: $\boldsymbol{E}=(E_x, 0, 0)$ belongs to Γ_2, $\boldsymbol{E}=(0, E_y, 0)$ to Γ_1.

$\psi(\boldsymbol{k}, \boldsymbol{r})$	$\psi_v \cdot \psi_c$	Φ_{nlm}	$\psi_v \cdot \psi_c \cdot \Phi$	χ_i	$\psi_v \cdot \psi_c \cdot \Phi \cdot \chi$	Visible for	Strength of absorption	Multiplet component
ψ_v: Γ_1 ψ_c: Γ_1	Γ_1	s, p_y: Γ_1	Γ_1	χ_1: Γ_1	Γ_1	$\boldsymbol{E} \perp \boldsymbol{H}$	very weak	singlet
				χ_2: Γ_1	Γ_1	$\boldsymbol{E} \perp \boldsymbol{H}$	weak	triplet
				χ_3: Γ_2	Γ_2	$\boldsymbol{E} \parallel \boldsymbol{H}$	weak	triplet
				χ_4: Γ_2	Γ_2	$\boldsymbol{E} \parallel \boldsymbol{H}$	weak	triplet

The selection rules for excitons in the Voigt geometry are given in Table VIII. Only mixed s-p_y states in the LS coupling limit are considered. It should be noted that for the states relating to the field-free triplet s states the listed strength of absorption also holds for $\boldsymbol{H}=0$. The oscillator strength of all other states disappears as indicated in Fig. 14 when $\boldsymbol{H}$ goes to zero.

5. – Discussion.

5·1. *The experiment.* – The magneto-optical absorption measurements which we interpret on the basis of the present theoretical considerations were carried out by BREBNER, HALPERN and MOOSER [7] at the National Magnet Laboratory in Boston, Mass. Experimental equipment, measuring procedures and investigated crystals—they were all grown by iodine transport [3]—are discussed in ref. [13]. In principle all measurements were carried out with light incident parallel to the c-axis, *i.e.* with the polarization vector $\boldsymbol{E} \perp c$. Because of the finite angular aperture of the optical system used and because of accidental misalignment of the samples small deviations from this incidence occurred. Transitions which are allowed only for light with a component of $\boldsymbol{E}$ along c, therefore, are also visible in some of the spectra.

The sample of β-GaSe whose exciton spectrum is reproduced in Fig. 9 was also obtained by iodine transport. Its structure was identified from the hexagonal shape of the growth spirals appearing on the (001)-surfaces. These hexagonal spirals are characteristic of the β-modification [3] which normally is found only in GaS. The identification was verified by X-ray diffraction.

Some reflectivity measurements with 45° incidence on the layer plane have since been carried out [45] to corroborate the polarization dependence of the optical transitions. They were made on c'eaved (001)-faces of large Bridgman grown crystals. A typical result of these measurements is shown in Fig. 8.

[45] CH. DEPEURSINGE and M. PY: Travail de diplôme, EPFL 1972, unpublished.

5·2. *Field-free case*: $\boldsymbol{H}=0$. – In Fig. 8 the ground state is reproduced of the exciton in a sample of γ-, ε-GaSe as observed in reflexion with light incident at 45° and with the polarization vector parallel ($\boldsymbol{E}\|$P.I.) and perpendicular ($\boldsymbol{E}\perp$P.I.) to the plane of incidence. For $\boldsymbol{E}\perp$P.I. a group of relatively

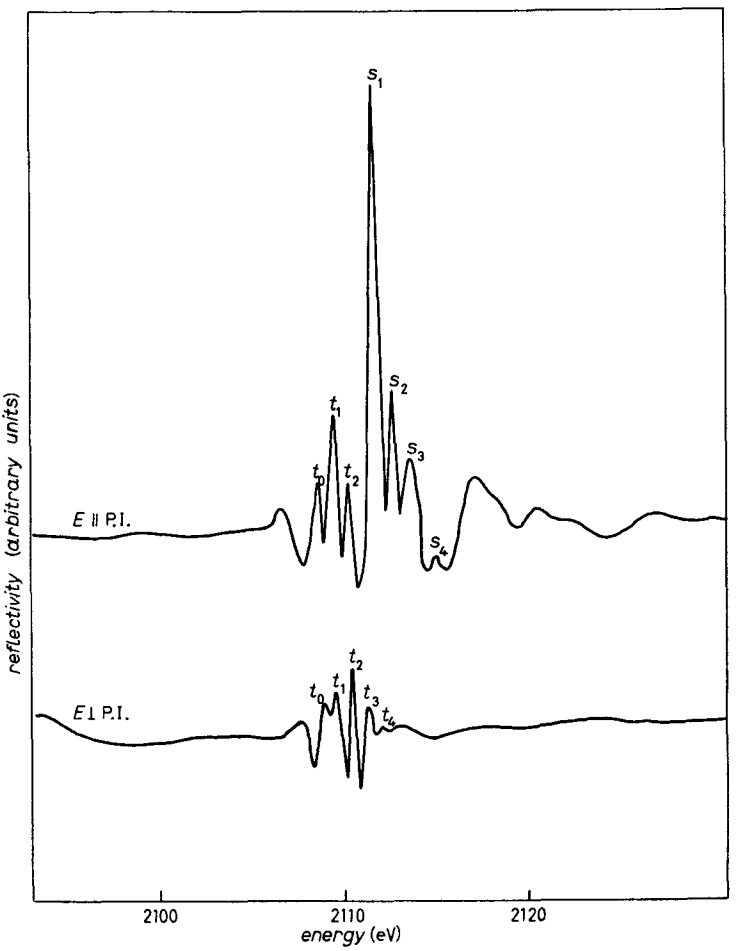

Fig. 8. – The fine structure of the exciton ground state in γ-, ε-GaSe at zero magnetic field. The measurements were taken with light incident at an angle of 45° with respect to the c-axis and with the polarization vector parallel ($\boldsymbol{E}\|$P.I.) and perpendicular ($\boldsymbol{E}\perp$P.I.) to the plane of incidence (after DEPEURSINGE and PY [45]).

weak lines t_i is observed. They represent some of the possible triplet fine-structure components $E^{(1s)}_{\Gamma_6}(A_5)$ induced by the stacking sequences A_5. As the plane of polarization is turned into the plane of incidence ($\boldsymbol{E}\|$P.I.) the polarization vector acquires a component along c and the singlet components $E^{(1s)}_{\Gamma_4}(A_5)$ marked s_i in the diagram become visible. Indeed, the transition into the singlet states Γ_4 now is allowed (see Table V), but that into the triplet states Γ_6

remains allowed by spin-orbit coupling only. The lines s_i therefore are much stronger than the corresponding lines t_i in spite of the fact that, because of the high refractive index ([46]) $n = 3$ of GaSe, the component of $\boldsymbol{E}$ perpendicular to c is still considerably longer than that parallel to it. The relative intensities of the lines s_i and t_i readily permit corresponding singlet and triplet components to be identified and thus to determine the singlet-triplet splitting for this geometry to be $\Delta E^{(1s)}_{\Gamma_4^- \Gamma_6}(A_5) = (1.9 \pm 0.1)$ meV.

The absorption measurements in the Faraday and Voigt geometries at $\boldsymbol{H} = 0$ (see Fig. 10 and Fig. 12, bottom curves) also show the singlet and triplet states, but because of the near perpendicular incidence only the largest of the singlet components is visible. The identification of the singlet is readily possible from its near independence of $\boldsymbol{H}$ (Fig. 10) and from its striking polarization dependence seen in Fig. 12 and 13. Within the experimental error the value $\Delta E^{(1s)}_{\Gamma_4^- \Gamma_6}(A_5) = (1.8 \pm 0.1)$ meV found from the absorption measurements is equal to that found in the reflexion measurements. As pointed out by BREBNER ([13]) the singlet observed in absorption has almost pure longitudinal character, a fact which incidentally accounts for its surprisingly high visibility ([47]) at near normal incidence. However, in the reflectivity measurements the singlet has mixed longitudinal and transversal character. We can therefore conclude that in the limited range of angles covered by the present experiments and within the accuracy of the measurements the singlet-triplet splitting does not depend on $\boldsymbol{K}$.

TABLE IX. – *Experimentally observed energies and ionization energies of the triplet s excitons in* GaSe.

Observed energy (eV)	Ionization energy $-E^{(ns)}_{ex}$ (meV)
$2.1098 \pm 0.5 \cdot 10^{-4}$	19.8 ± 0.1
2.1245	5.0
2.1272	2.3

The experimental values averaged over six measurements of the lowest three exciton s levels at 1.7 °K are given in Table IX in which the ground-state energy is that of the predominant triplet. If we assume the differences between the gap energy E_g and the listed levels to be proportional to $1/n^2$, the value $E_g = (2.1295 \pm 0.5) \cdot 10^{-4}$ eV was obtained which served to evaluate the ionization energies $E^{(ns)}_{ex}$. According to DÉVERIN ([21]) the effective Rydberg $-E^{(1)}_{0ex}$ defined by eq. (15) and the reduced effective mass μ_x can be derived

([46]) J. L. BREBNER and J. A. DÉVERIN: *Helv. Phys. Acta*, **38**, 650 (1965).
([47]) J. J. HOPFIELD and D. G. THOMAS: *Journ. Phys. Chem. Sol.*, **12**, 276 (1960).

from $E_{ex}^{(1s)}$ and $E_{ex}^{(2s)}$ as follows:

$$-E_{0ex}^{(1)} = R\cdot\frac{\mu_x}{m}\cdot\frac{1}{\varepsilon_x\varepsilon_z} = \frac{-E_{ex}^{(1s)}}{f^{00}(\alpha)-1} = \frac{-4E_{ex}^{(2s)}}{f^{00}(\alpha)-1}, \tag{55}$$

where

$$f^{00}(\alpha) = \frac{1}{\sqrt{\alpha-1}}\cdot\ln\frac{\sqrt{\alpha}+\sqrt{\alpha-1}}{\sqrt{\alpha}-\sqrt{\alpha-1}}. \tag{56}$$

With the value $\alpha = \mu_x\varepsilon_x/\mu_z\varepsilon_z = 1.8$ determined from the magneto-absorption measurements (Subsect. 5˚3.2) $f^{00}(1.8) = 1.8$, and taking $\varepsilon_x = 10.2$ and $\varepsilon_z = 7.6$ in accordance with LEUNG *et al.* ([48]) one has

$$-E_{0ex}^{(1s)} = (24.8 \pm 0.6)\,\text{meV} \quad \text{and} \quad \frac{\mu_x}{m} = 0.14 \pm 0.05\,. \tag{57}$$

These results as well as those derived below depend on our choice of the ε_x and ε_y values. The question as to how well these dielectric constants describe the exciton remains of course open.

If we introduce μ_x/m in eq. (16), the radius of the zeroth-order $1s$ envelope is found to be $a_{0ex}^{(1s)} = 32$ Å, a value which is compatible with our earlier findings that the $1s$ exciton extends over five layers (40 Å).

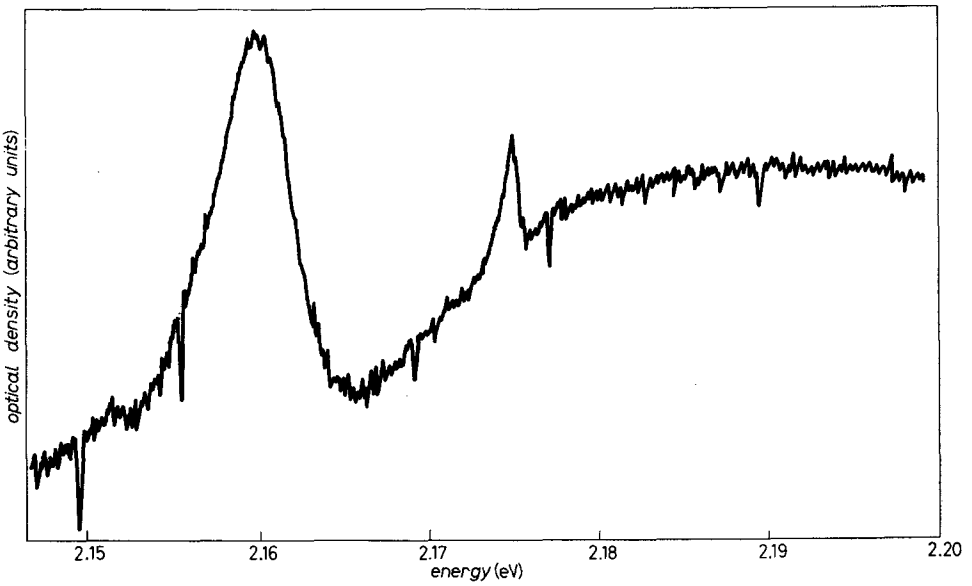

Fig. 9. – The exciton spectrum of β-GaSe at zero magnetic field and with light incident along c.

([48]) P. C. LEUNG, G. ANDERMANN, W. G. SPITZER and C. A. MEAD: *Journ. Phys. Chem. Sol.*, **27**, 849 (1966).

The exciton spectrum of a transport reacted crystal of β-GaSe is shown in Fig. 9. The sharp inverted peaks near 2.150 eV and 2.156 eV belong to the neon calibration spectrum. Compared to the γ-, ε-exciton levels those of the β-modification are displaced by 50 meV towards higher energies. However, the difference between the $n=1$ and $n=2$ levels is the same as in γ-, ε-GaSe. We may therefore conclude that within experimental accuracy the ionization energies of the excitons are the same in all modifications. Unlike in the γ-, ε-samples the ground state in the β-crystals is not split into stacking fault components. This is understandable because the β-structure does not admit low-energy glide stacking faults. The strain-releasing mechanism involving such faults therefore is not operative and the residual strain due to the (possible) instability of the β-modification leads to the rather smeared-out lines shown in Fig. 9.

5·3. *The exciton in a magnetic field.*

5·3.1. The Faraday geometry. In Fig. 10 a series of absorption spectra in Faraday geometry is reproduced which correspond to different magnetic fields. The sharp inverted peak at 2.1178 eV appearing in all of them is a neon emission line serving as calibration mark. The topmost spectrum was taken with left circularly polarized light (l.c.p.), all the others with right circularly polarized light (r.c.p.).

Since the observed ground- and first excited states ($1s$ and $2s$) do not carry an orbital moment, the shifts between corresponding r.c.p. and l.c.p. lines are entirely due to the spin term which is nonzero for the triplet states whose spin components S_z are ± 1. Evaluating the experimental data for the $1s$ and $2s$ triplet states Γ_2 and Γ_3 (Table VII) and for fields up to 90 kG one obtains a splitting per unit field of

$$\frac{\Delta E_{\text{spin}}}{H_z} = (1.6 + 0.1)\cdot 10^{-2}\,\frac{\text{meV}}{\text{kG}}\,,$$

from which according to (39) the z-component of the exciton g-factor is found to be

$$(58) \qquad g_z = \frac{2mc}{e\hbar}\cdot\frac{H_7(S_z=+1)-H_7(S_z=-1)}{H_z} = \frac{\Delta E_{\text{spin}}}{H_z}\cdot 1.7\cdot 10^{-2} = 2.7 \pm 0.2\,.$$

In Fig. 11 the fan chart corresponding to the $1s$ and $2s$ states of symmetry Γ_2, Γ_3 (triplet) and Γ_4 (singlet) is shown. The points mark experimental data. The curves were calculated from (37) and (39) with

$$(59) \qquad \sigma = 4.3\cdot 10^{-5}\,\frac{\text{meV}}{(\text{kG})^2}$$

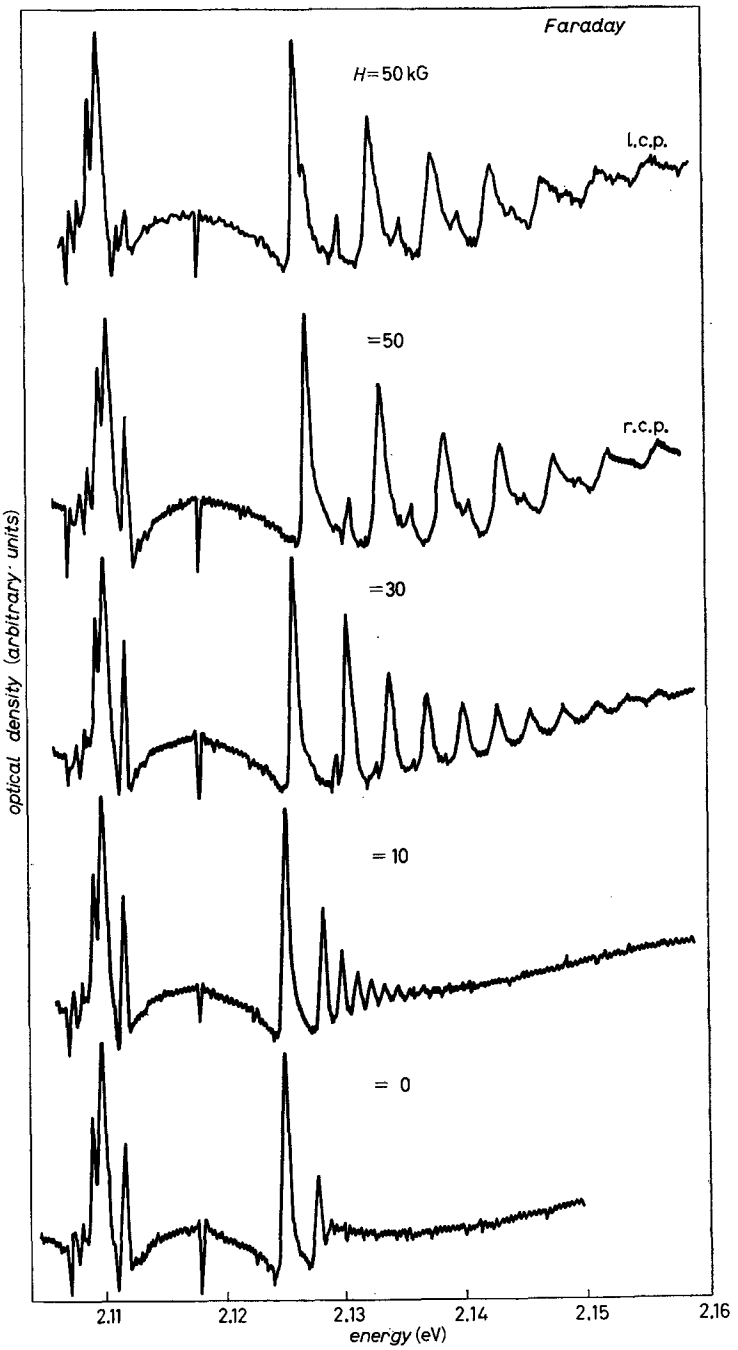

Fig. 10. – The magneto-absorption spectrum of γ-, ε-GaSe in Faraday geometry. The uppermost spectrum was obtained in left circularly polarized light (l.c.p.), all the others in right circularly polarized light (r.c.p.).

and with $g_z = 2.7$, and they were fitted to experiment at $H_z = 0$. The reduced effective mass $\mu_x/m = 0.13$ obtained according to (38) from this σ value is in excellent agreement with that (57) derived from the ionization energies.

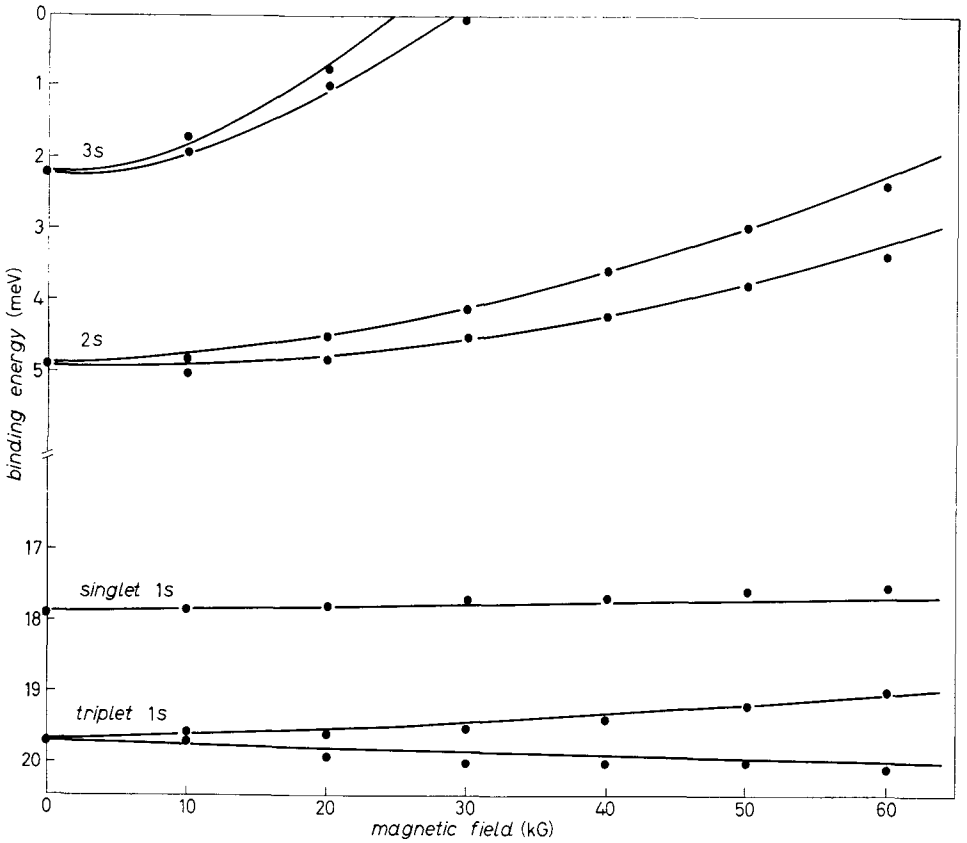

Fig. 11. – The magnetic-field dependence of the exciton states $n = 1, 2$ and 3 taken from Fig. 10. The curves were calculated according to (37) and (39) and fitted at $\boldsymbol{H} = 0$.

Also plotted in Fig. 11 are the low-field experimental data corresponding to the Γ_2, Γ_3 states whose principal quantum number is $n = 3$. These states are no longer pure s, but have a considerable admixture of d_0 character (see ref. ([21])). Nevertheless, the curves shown in Fig. 11 which were calculated with $g_z = 2.7$ and with

$$\langle 3s|H_4'|3s\rangle = 69\sigma H_z^2 \tag{60}$$

fit the experiment quite well up to 30 kG. At high fields, however, a marked discrepancy is observed: the diamagnetic shift calculated for 80 kG exceeds the experimental one by more than 100 %.

The singlet nature of the state whose zero-field ionization energy is 17.9 meV is clearly recognizable from Fig. 11. The magnetic field only affects its energy via the diamagnetic term: there is no spin splitting. It should be noted in this connection that if in Fig. 10 the singlet state is best visible for r.c.p., it is still clearly recognizable for l.c.p. and any possible spin splitting would therefore have been detected.

The good characterization of the multiplet nature of the exciton states is strong evidence for the weak spin-orbit coupling in GaSe. It is not surprising, therefore, that of the selection rules discussed in Subsect. 4·2.3 those relating to weak spin-orbit coupling (Table V) give a better description of the observed polarization dependence of the field-free Γ_4 and Γ_6 s excitons than those relating to strong spin-orbit coupling (Table VI). For strong coupling, absorption (and reflexion) of the Γ_4 exciton with $\boldsymbol{E}\|c$ and of the Γ_6 exciton with $\boldsymbol{E}\perp c$ should both be strong and this is in contradiction with experiment (see also ref. [24.26]).

5·3.2. The Voigt geometry. A series of absorption spectra taken in Voigt geometry at different magnetic fields and with $\boldsymbol{E}\perp\boldsymbol{H}$ is shown in Fig. 12. Similar spectra taken on the same sample but with $\boldsymbol{E}\|\boldsymbol{H}$ are reproduced in Fig. 13. According to the selection rules listed in Table VIII the states visible in Fig. 12 are the field-free Γ_6 triplets which with increasing $\boldsymbol{H}$ give way to the Γ_1 triplets. For $\boldsymbol{H}\neq 0$ the Γ_1 singlets should also become visible. However, it should be noted that the $1s$ singlet is visible even at $\boldsymbol{H}=0$ and its strength of absorption does not depend on $\boldsymbol{H}$. Its visibility therefore is essentially due to the slight off-normal incidence mentioned in Subsect. 5·1. The influence of magnetic fields as high as 100 kG upon the transition probability into the $1s$ exciton states is expected to be very small. The lines visible in Fig. 13 are the Γ_2 triplets.

It follows from eq. (37) and (48) that a comparison of the diamagnetic shifts corresponding to the two investigated geometries allows the reduced effective-mass ratio μ_x/μ_z to be evaluated. However, we have seen in Subsect. 4·3.2 that in the Voigt geometry the magneto-Stark term mixes the $2s$ and $2p_y$ states. Before the secular equation corresponding to the matrix (54) has been evaluated the comparison is therefore possible only for the $1s$ states and because of the smallness of their shifts gives rather inaccurate results. From measurements in fields as high as 90 kG one finds

$$\frac{\langle 1s|H_4'|1s\rangle_{\text{Voigt}}}{\langle 1s|H_4'|1s\rangle_{\text{Farad}}}=\frac{\mu_x}{\mu_z}=1\pm 0.2\,. \tag{61}$$

The most remarkable feature of Fig. 12 and 13 is the appearance with increasing $\boldsymbol{H}$ of new absorption lines immediately below the $2s$ states. These lines are attributed to the $2p_y$ states which via the $\boldsymbol{A}\cdot\boldsymbol{K}$ term acquire rapidly

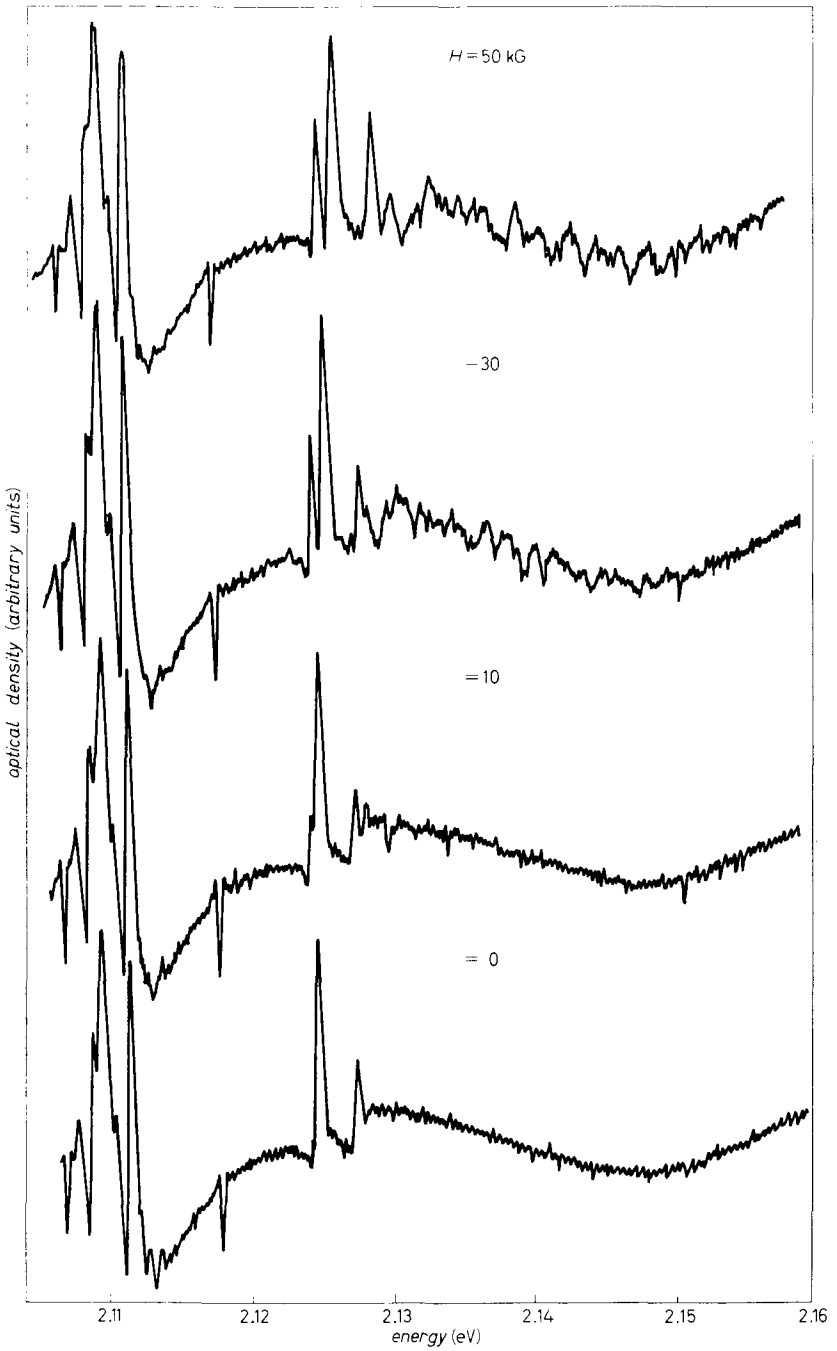

Fig. 12. – The magneto-absorption spectrum of γ-, ε-GaSe in Voigt geometry for $\boldsymbol{E} \perp \boldsymbol{H}$, $\boldsymbol{H} \perp c$.

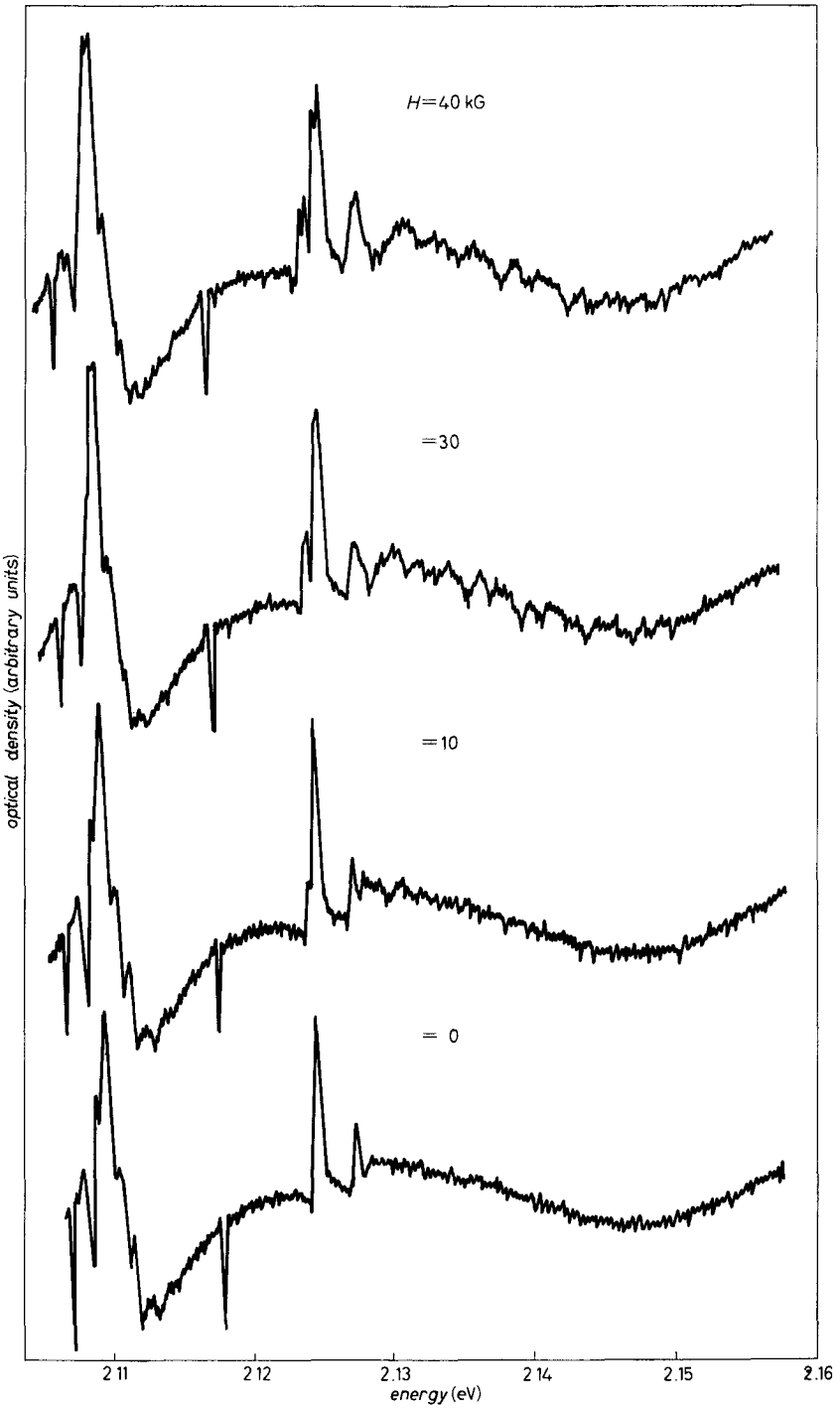

Fig. 13. – The magneto-absorption spectrum of γ-, ε-GaSe in Voigt geometry for $\boldsymbol{E} \parallel \boldsymbol{H}$, $\boldsymbol{H} \perp c$.

increasing s character. Extrapolating their position to $\boldsymbol{H}=0$ one finds the ionization energy of the $2p_{\pm 1}$ state

$$-E_{ex}^{(2p_{\pm 1})} = (5.5 \pm 0.1)\ \text{meV}\,. \tag{62}$$

This value together with that of the ionization energy $E_{ex}^{(2s)} = 5$ meV taken from Table IX allow the anisotropy parameter $\alpha = \mu_x \varepsilon_x / \mu_z \varepsilon_z$ to be determined. Indeed, according to DÉVERIN ([21]) one has

$$\frac{E_{ex}^{(2p_{\pm 1})} - E_{ex}^{(2s)}}{E_{ex}^{(2s)}} = 0.1 = \frac{\frac{3}{2} f^{11}(\alpha) - f^{00}(\alpha)}{f^{00}(\alpha) - 1}\,, \tag{63}$$

which with the $f^{00}(\alpha)$ defined in (56) and with

$$f^{11}(\alpha) = \frac{1}{\sqrt{\alpha - 1}} \left[1 + \frac{1}{2(\alpha - 1)}\right] \ln\left(\frac{\sqrt{\alpha} + \sqrt{\alpha - 1}}{\sqrt{\alpha} - \sqrt{\alpha - 1}}\right) - \frac{\sqrt{\alpha}}{\alpha - 1} \tag{64}$$

gives

$$\alpha = \frac{\mu_x \varepsilon_x}{\mu_z \varepsilon_z} = 1.8\,. \tag{65}$$

With the dielectric constants ε_x and ε_z given in ref. ([48]) one thus obtains another value for the reduced effective-mass ratio

$$\frac{\mu_x}{\mu_z} = 1.3 \pm 0.2\,. \tag{66}$$

We have seen in Subsect. 4·3.2 that the energies and the percentages of s character of the mixed s and p states can be calculated from the 3×3 matrix (54). By fitting the solutions of the corresponding secular equation to experiment—the percentage of s character was determined from the ratio of the squared peak values of the observed absorption lines—the following results were obtained:

$$\alpha_D = \sigma \frac{\mu_x}{\mu_z} = 4.1 \cdot 10^{-5} \frac{\text{meV}}{(\text{kG})^2}\,, \tag{67}$$

$$i\alpha_L = \frac{e\hbar}{2\mu_x' c} \cdot b^+ = \frac{e\hbar}{4\mu_x' c} \left(\frac{\mu_z}{\mu_z}\right)^{\frac{1}{2}} \left(\frac{\mu_x'}{\mu_z'} + \frac{\mu_x}{\mu_z}\right) = 7 \cdot 10^{-3} \frac{\text{meV}}{\text{kG}} \tag{68}$$

and

$$\alpha_{MS} = \frac{e\hbar}{2M_z c} a_{0ex}^{(1)} K_z = 1.4 \cdot 10^{-2} \frac{\text{meV}}{\text{kG}}\,. \tag{69}$$

The theoretical curves calculated with these parameter values are drawn in Fig. 14 in which the experimental results are marked by points. The dashed curve gives the H-dependence of the state correlating with p_z. This state is not seen in experiment.

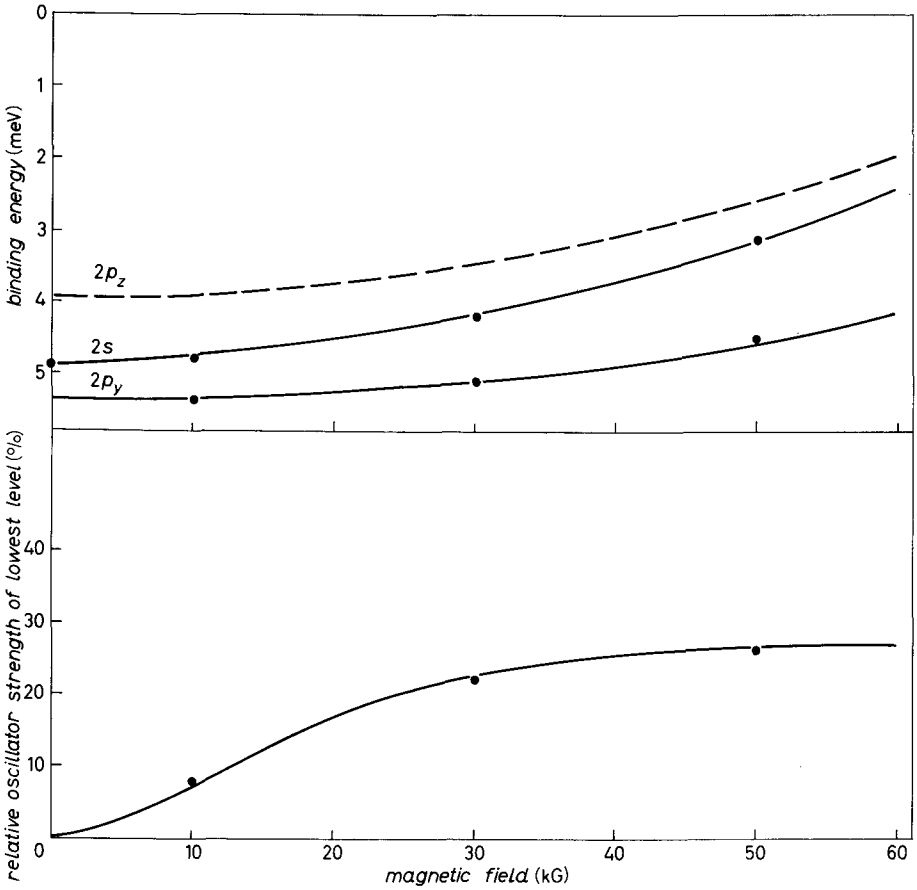

Fig. 14. – The magnetic-field dependence of the mixed $2s$, $2p$ levels and of the relative oscillator strength of the lowest $n=2$ level as derived from Fig. 12. The curves are calculated from the matrix (54).

With (59) α_D gives yet a third value for the reduced effective-mass ratio:

$$\frac{\mu_x}{\mu_z} = \frac{\alpha_D}{\sigma} = 0.95 . \tag{70}$$

Introducing $\mu_x/\mu_z = 1$ in (68) one readily finds

$$\frac{m}{\mu_x'} + \frac{m}{\mu_z'} = 2.4 . \tag{71}$$

TABLE X. – *Effective electron and hole masses in* GaSe.

	Component	
	x	z
m_e^*	$0.17\,m$	$0.3\ m$
m_h^*	$0.8\ m$	$0.2\ m$
μ	$0.14\,m$	$0.12\,m$
μ'	$4.6\ m$	$-1.7\ m$

This value is in good agreement with that $m/\mu_x' + m/\mu_z' = 2.9$ derived from the set of effective electron and hole masses listed in Table X. The data contained in this Table were obtained by OTTAVIANI *et al.* [49] from a critical analysis of recent transport measurements and from the data on μ_x and μ_x/μ_z found in the present paper.

From (69) the component K_z of the exciton wave vector can be evaluated at

$$K_z = 7.3 \cdot 10^{-2} \frac{M_z}{m} \text{ Å}^{-1} . \tag{72}$$

Comparing this value with that $K_z = 2\pi n/\lambda = 3.2 \cdot 10^{-3}$ Å^{-1} derived from the wavelength $\lambda = 5\,835$ Å of the absorbed light and from the corresponding refractive index [46] $n = 3$ one finds a rather low value $M_z = 5 \cdot 10^{-2}\,m$ for the total exciton mass along z. However, it should be noted that, since the exciton lines are regions of anomalous dispersion, the appropriate refractive index may well exceed the one used above by a factor of ten. Moreover, the value $M_z = 0.5\ m$ obtained from Table X is indeed surprisingly low.

Finally we use the Γ_2 triplet splitting visible at 50 kG in Fig. 13 to determine the x-component of the exciton g-factor. From the $1s$ and the mixed $2s$-$2p_y$ states—within experimental accuracy they all show the same splitting—and from experiments extending to fields as high as 90 kG we find

$$g_x = 1.9 \pm 0.15 . \tag{73}$$

6. – Conclusion.

In conclusion we would like to say that on the basis of new band calculations a detailed interpretation of the optical valence-to-conduction band transitions in GaSe is possible. The mixing of two nondegenerate valence

[49] G. OTTAVIANI, C. CANALI, PH. SCHMID, M. SCHLÜTER, E. MOOSER and R. MINDER: in preparation.

bands induced by weak spin-orbit coupling furnishes a very satisfactory explanation for the weak absorption observed at the fundamental edge for light polarized perpendicularly to the c-axis. This weak absorption has rendered possible measurements for energies well beyond the ionization limit of the exciton and the data collected in this way have given rise to a series of most interesting theoretical considerations ([8-12]).

Within the framework of the ellipsoidal effective-mass approximation a consistent interpretation can be given of the exciton spectra and of the influence upon them of magnetic fields parallel and perpendicular to c. Because of the weakness of the spin-orbit coupling a considerable exchange splitting of the ground state is observed. A detailed investigation of the dependence of this splitting on the angle of incidence which is as yet lacking should furnish information about the spatial dispersion of the mixed longitudinal-transversal excitons. The $\boldsymbol{A}\cdot\boldsymbol{K}$ induced s-p_y mixing permits one to ascertain that the excitons in GaSe are mobile perpendicular to the plane of the layers. This is in contradiction with an earlier interpretation ([25]) of the fine structure of the exciton ground state. At the time the fine structure was taken as evidence for the binding of excitons to individual layers. As shown here this hypothesis is not necessary for the understanding of the fine structure.

In the light of the interest in layer structures which has been steadily increasing in recent years the ease with which excitons move across the layers is perhaps the most remarkable result of the present analysis. This ease is not only evident from the nonzero magneto-Stark term but also from the values of the anisotropy parameter and of the reduced effective masses and their ratio. From all this evidence we conclude that if some of the bands in GaSe have essentially two-dimensional character as seen from Fig. 2, those determining the optical (and electrical) properties are definitely three dimensional.

● RIASSUNTO (*)

Si interpretano gli spettri di assorbimento e di riflessione del GaSe in prossimità della « gap » fondamentale facendo uso di calcoli della struttura a bande basati sull'impiego di pseudopotenziali. Si ottengono regole di selezione per le transizioni ottiche dirette tra la banda di valenza e quella di conduzione. Si ricorre al mescolamento della banda di valenza determinato dall'accoppiamento spin-orbita per spiegare la bassa probabilità di transizione che si osserva impiegando luce polarizzata perpendicolarmente all'asse c del cristallo. Si discutono gli spettri degli eccitoni associati alla « gap » diretta, nell'approssimazione di masse effettive ellissoidali. Si aggiungono termini di correzione per tener conto della separazione di scambio che si osserva nello stato fondamentale degli

(*) *Traduzione a cura della Redazione.*

eccitoni. Si considerano sia spettri liberi da campi esterni sia spettri modificati dalla presenza di campi magnetici paralleli e perpendicolari a c. L'effetto Stark magnetico, che dà origine alla sovrapposizione degli stati $2s$ e $2p_y$ e che in tal modo rende possibile l'osservazione dello stato $2p_y$, consente di determinare il parametro di anisotropia. Sia il valore di tale parametro sia quelli delle componenti, parallele e perpendicolare a c, delle masse effettive ridotte mostrano che gli stati elettronici del GaSe sono pressoché isotropi. Ciò è in buon accordo con i risultati dei calcoli della struttura a bande basati sull'impiego di pseudopotenziali e che mostrano charamente il carattere tridimensionale della banda di valenza e di quella di conduzione.

Резюме не получено.

Direttore responsabile: GIULIANO TORALDO DI FRANCIA

Stampato in Bologna dalla Tipografia Compositori coi tipi della Tipografia Monograf
Questo fascicolo è stato licenziato dai torchi il 31-X-1973